Studies of DNA Polymerases Involved in DNA Repair and Lesion Bypass

Honors Research Thesis

Presented in partial fulfillment of the requirements for graduation *with honors research distinction* in Biochemistry in the undergraduate colleges of The Ohio State University

by

Laura Elizabeth Sanman

The Ohio State University

June 2011

Project Advisor: Dr. Zucai Suo, Department of Biochemistry

Contents

Introduction

Genomic DNA is under constant stress from both endogenous and exogenous sources. Factors such as UV light, chemotherapeutic agents, and even normal metabolic activities can all damage DNA by creating lesions; nitrogenous base alterations that include crosslinking, addition of covalent adducts, and spontaneous base loss. All forms of DNA damage are potentially detrimental because they hinder the cell's ability to replicate DNA efficiently and accurately. Fortunately, the cell has many methods to minimize the effects of DNA damage. The damage can either be repaired or, if an unrepaired lesion stalls DNA replication, tolerated through lesion bypass. Because these pathways are the means by which genome integrity is maintained, they are very important to thoroughly understand[1]. The studies reported herein concern two families of enzymes involved in the complex DNA damage response; the X- and Y-families of DNA polymerases.

Chapter 1 focuses on the X-family DNA polymerases, which are primarily implicated in DNA repair pathways[2]. Two X-family enzymes were selected and their ability to fill gaps in DNA characterized. Gap filling is an essential step of base excision repair, therefore this study contributed to knowledge of the two polymerases' putative biological roles. The results of this study were also published in DNA Repair[3]. In Chapters 2 and 3, the focus switches to the Y-family DNA polymerases, which are primarily implicated in lesion bypass[4]. These chapters report the mutagenic profile of *cis-syn* cyclobutane thymine dimer and cisplatin-dGpG lesion bypass by the human Y-family DNA polymerases as well as a model Y-family DNA polymerase from *Sulfolobus solfataricus*. It should be noted that the projects discussed in Chapters 2 and 3 are ongoing and that the results reported are preliminary.

In this thesis, I discuss the three projects in which I had the most involvement during my time in Dr. Suo's laboratory. This being said, each project was part of a larger collaborative effort and was undertaken with the guidance and assistance of other members of the lab. Therefore, as I discuss the results of each project I will try to highlight my own contribution and to acknowledge the hard work of others.

Chapter 1: An Investigation of the Gap-Filling Activity of Human DNA Polymerases Lambda and Beta

Background

As stated in the Introduction, the cell's response to DNA damage is very complex. All lesions are not repaired in the same way. In fact, there are several pathways through which the cell can repair damaged DNA. One of these pathways is base excision repair (BER). It is the predominant way in which single-base DNA lesions are repaired in mammals[5]. In base excision repair, the damage is first recognized by a lesion-specific DNA glycosylase, which cleaves the glycosidic bond attaching the damaged nitrogenous base to its deoxyribose, generating an apurinic or apyrimidinic (AP) site. The phosphodiester backbone of DNA is then cleaved adjacent to the lesion by AP endonuclease I. The resulting gap in DNA is filled by a DNA polymerase, which also removes the 5'-deoxyribose phosphate (dRP) of the downstream strand with its dRP lyase domain. Finally, the phosphodiester backbone is sealed by a DNA ligase. Interestingly, the gap-filling step of BER can be accomplished in two ways - termed short-patch BER (SP-BER) and long patch BER (LP-BER). In SP-BER, the DNA polymerase incorporates only one nucleotide. In LP-BER, 2-10 nucleotides are incorporated, displacing the downstream strand. The downstream strand is then removed by flap endonuclease I[6].

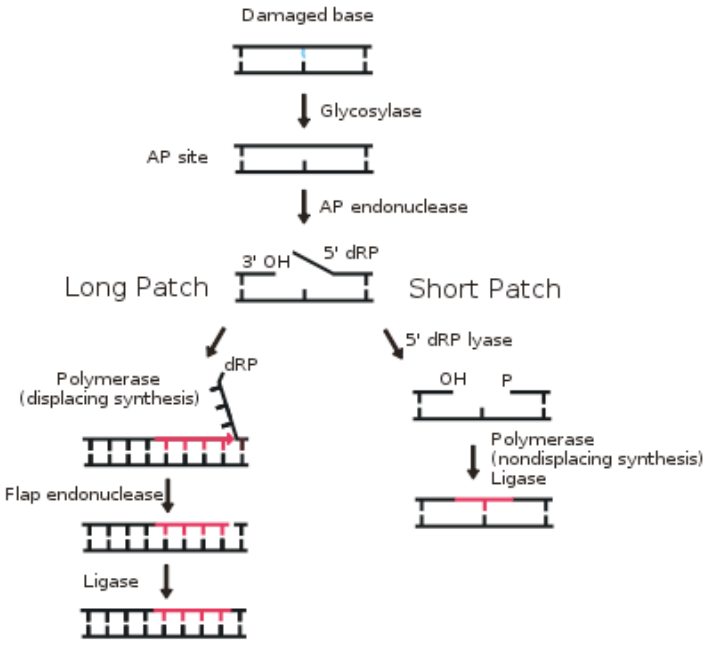

Figure 1. A scheme of the general BER pathway[6].

In this study, we focused on the gap-filling step of BER. To perform this step, the DNA polymerase must be able to catalyze gap-filling DNA synthesis and must contain a dRPase domain. The two X-family DNA polymerases in this study, human DNA polymerase beta (hPolβ) and human DNA polymerase lambda (hPolλ), possess these abilities[7]. hPolβ has been proven to perform SP-BER *in vivo*[8], and is there is also evidence that it functions in LP-BER[9]. We chose to study hPolλ because it meets the above criteria for BER function and it shares 34% sequence similarity with hPolβ[10]. hPolλ is also structurally similar to hPolβ, though hPolλ possesses N-terminal BRCT and proline-rich domains[11]. Additionally, it has been proposed that hPolλ plays a complementary and/or supporting role to hPolβ *in vivo*[7]. Motivated by this information, we completed a detailed pre-steady state kinetic analysis of gap-filling synthesis by hPolλ and hPolβ on DNA containing 1-10 nucleotide gaps. The goals of this study were as follows: 1) to determine the effect of gap size on DNA polymerase fidelity and incorporation

efficiency, 2) to observe the effect of hPolλ's N-terminal BRCT and proline-rich domains on its ability to perform gap filling synthesis and, 3) to compare the gap-filling activities of hPolβ and hPolλ.

Methods

Materials: The following reagents were purchased for this project: OptiKinase™ from USB Corporation, deoxyribonucleotide-5'-triphosphates from GE Healthcare, [γ-^{32}P]ATP from MP Biomedicals, Bio-Spin 6 columns from Bio-Rad Laboratories, synthetic deoxyribonucleotides including a primer 21-mer, 5'-phosphorylated 19-mer, and template 41- to 50-mers from Integrated DNA Technologies. Wildtype human DNA polymerase lambda (hPolλ), two N-terminal truncations of human DNA polymerase lambda (dPolλ, tPolλ), and human DNA polymerase beta (hPolβ) were expressed and purified for earlier studies as described previously[23].

Construction of gapped DNA substrates: All synthetic deoxyribonucleotides purchased from Integrated DNA Technologies were purified using polyacrylamide gel electrophoresis and subsequently extracted and desalted for use. Concentration of the various deoxyribonucleotides was determined using UV spectroscopy at 260 nm. Deoxyribonucleotides were purified by various members of the Suo lab including two purified personally. David Beyer is to be thanked especially for the extensive DNA purification work he did for this project. The primer 21-mer was radiolabeled with [γ-^{32}P]ATP using OptiKinase™. Unreacted [γ-^{32}P]ATP was removed using Bio-Spin 6 size exclusion columns. Radiolabeling and removal of unreacted [γ-^{32}P]ATP were both completed according to manufacturer's directions. Gapped DNA substrates were constructed by mixing 5'-[^{32}P]-radiolabeled 21mer, template 41- to 50-mer, and the

complementary downstream 19-mer at a 1:1.15:1.25 molar ratio, respectively. This mixture was denatured by heating at 95C for 5 minutes, and annealing of deoxyribonucleotides was accomplished by cooling the mixture slowly to room temperature. The sequences of all annealed gapped substrates can be found in Appendix 1, Table 1.

Single nucleotide incorporation assays: All kinetic assays on hPolλ, tPolλ, and dPolλ were performed in optimized buffer "L"; 50 mM Tris-Cl pH 8.4 at 37˚C, 5 mM $MgCl_2$, 100 mM NaCl, 0.1 mM EDTA, 5 mM dithiothreitol, 10% glycerol, and 0.1 mg/mL bovine serum albumin. All kinetic assays on hPolβ were performed in optimized buffer "B"; 50 mM Tris-Cl pH 7.8 at 37˚C, 5 mM $MgCl_2$, 50 mM NaCl, 0.1 mM EDTA, 5 mM dithiothreitol, 10% glycerol, and 0.1 mg/mL bovine serum albumin. The listed concentrations are indicative of final concentrations after mixing all reaction components. Kinetic assays were performed at 37˚C. To begin each reaction, a pre-incubated solution containing radiolabeled gapped substrate and hPolλ (120 nM), tPolλ (120 nM), dPolλ (120 nM) , or hPolβ (300 nM) in the appropriate buffer was mixed with increasing concentrations of a single nucleotide (0.2-1500 μm). At various time points, aliquots of the reaction mixture were removed and quenched in EDTA to a final [EDTA] of 0.37 M. Assays were either done by hand or, if too fast, using a rapid chemical-quench flow apparatus (KinTek). Reaction products were separated using 17% acrylamide 8M urea sequencing gel electrophoresis.

The resolved bands were imaged using a Typhoon TRIO (GE Healthcare) and product intensity quantified using ImageQuant. By plotting [Product] vs. time and using KaleidaGraph (Synergy Software) to generate nonlinear curvefits, k_{obs} of nucleotide incorporation was determined for each [dNTP] using Equation 1 (Figure 2).

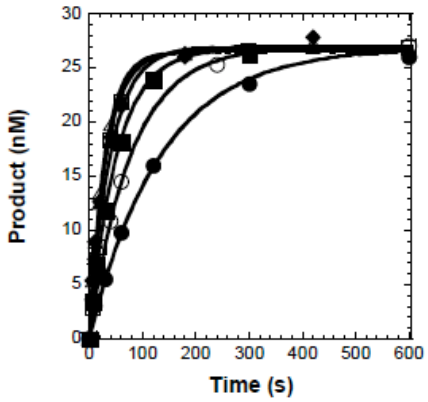

Figure 2: Relationship of Product Formation and Time. Each time course was fit using Equation 1 to calculate a k_{obs}.

Plotting the k_{obs} vs. [dNTP] and application of Equation 2 generated apparent k_p and K_D for incorporation of a single nucleotide on a specific gapped DNA substrate by either hPolλ, tPolλ, dPolλ, or hPolβ (Figure 3).

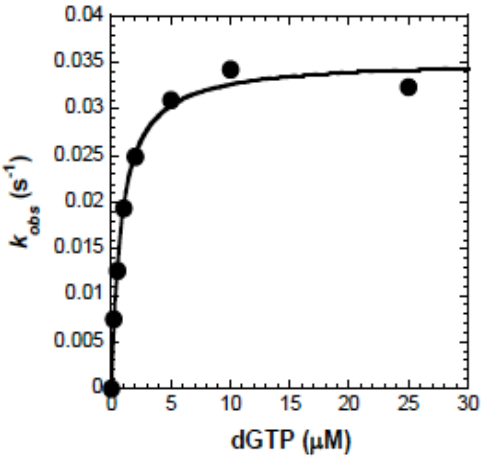

Figure 3: Relationship of k_{obs} and Nucleotide Concentration. The curve was fit using Equation 2 to yield a k_p and K_D.

When measuring both the k_p and K_D of correct and incorrect nucleotide incorporation, fidelity was calculated using Equation 3 in order to quantify the DNA polymerase's likelihood of correct incorporation. Pre-steady state kinetic assays were performed by myself, Lindsey Pack, and Jessica Brown, with L.P. and J.B. performing all of the assays requiring use of the rapid chemical-quench flow apparatus. Quantitation, data analysis, and data interpretation were shared.

$$[\text{Product}] = A[1-\exp(-k_{obs}t)] \quad \text{Equation 1}$$

$$k_{obs} = k_p[\text{dNTP}]/\{[\text{dNTP}]+K_D\} \quad \text{Equation 2}$$

$$\text{Fidelity} = [(k_p/K_D)_{incorrect}]/[(k_p/K_D)_{correct} + (k_p/K_D)_{incorrect}] \quad \text{Equation 3}$$

Results

The effect of gap size on DNA polymerase efficiency and fidelity:

a. hPolλ: We determined the k_p, K_D, incorporation efficiency, and fidelity of nucleotide incorporation by hPolλ under single turnover conditions on primer/template DNA substrates and DNA substrates containing gaps from 1-10 nucleotides. For example, we measured dGTP incorporation opposite template dC on 21-19/41mer single nucleotide gapped DNA substrate. A hyperbolic dependence on the observed rate constant (also signified k_{obs} as in Equation 1) was observed with increasing [dGTP]. From this, the maximum rate constant of pyrophosphorolysis (k_p) was determined to be 2.7 ± 0.1 s^{-1}, and the apparent equilibrium dissociation constant (K_D) for dGTP was determined to be 1.9 ± 0.2 μM. This leads to a calculated incorporation efficiency of 1.4 $\mu M^{-1}s^{-1}$. Ratio of the incorporation efficiency with 2-10 nucleotide gaps to incorporation efficiency at a gap size of one was also calculated. Finally, fidelity of each misincorporation was calculated as described in the Methods. A complete summary of the kinetic parameters obtained

is provided in Appendix 1, Table 2. The following is a summary of the notable results and our observations:

In brief, the presence of a downstream strand on the single nucleotide gapped DNA substrate increased the incorporation efficiency by 33-fold compared to primer/template DNA. This suggested that there is a gap size after which the downstream strand has minimal impact on gap-filling ability. To test this observation, 2-10 nucleotide gapped substrates were created by inserting bases into the DNA template, keeping the template 21-mer and downstream 19-mer constant. Nucleotide incorporation efficiency remained relatively constant until a gap size of 10, at which incorporation efficiency dropped 38-fold. This is comparable to the incorporation efficiency on primer/template DNA substrate, meaning that hPolλ has a maximum gap size of 9 nucleotides for efficient nucleotide incorporation (Figure 4).

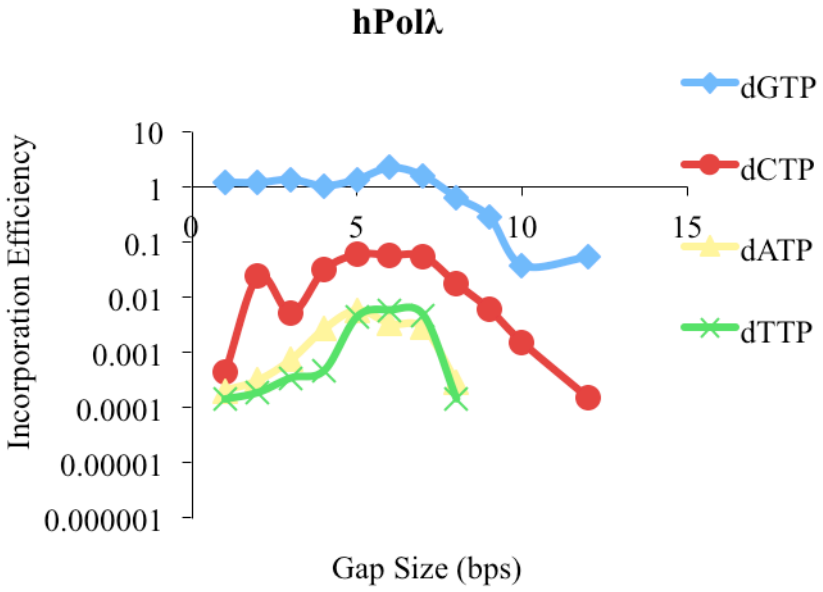

Figure 4. Effect of gap size on the incorporation efficiency of hPolλ. The points beyond a gap size of 10 indicate incorporation efficiency on primer/template DNA substrate.

Interestingly, dCTP was the preferred misincorporation for all gap sizes. In addition, the efficiency of dCTP incorporation increased 7- to 41-fold as the gap size widened from 2-8 nucleotides. dATP and dTTP, while not incorporated as efficiently as dCTP, also showed increased incorporation efficiency as gap size increased. This demonstrated an overall decrease in the fidelity of hPolλ as gap size increased.

In summary, hPolλ maintained nucleotide incorporation efficiency on 1-9 nucleotide gaps while showing an overall decrease in fidelity. Low polymerase fidelity is not ideal for maintenance of genome integrity, making hPolλ a poor choice for LP-BER. However, we could not rule out hPolλ's involvement in LP-BER without comparing it to a strong LP-BER

candidate. Therefore, we performed similar single-turnover kinetic studies on the gap-filling activity of hPolβ.

b. hPolβ: Kinetic parameters including k_p, K_D, incorporation efficiency, incorporation efficiency ratio, and fidelity were determined under single turnover conditions. Kinetic assays were performed on primer/template DNA and DNA containing 1, 2, 5, 7, and 10 nucleotide gaps. A complete summary of the kinetic parameters obtained is provided in Appendix 1, Table 4. Overall, the trends in kinetic parameters obtained were notably different than those obtained from hPolλ. For example, there was only a 3-fold difference in nucleotide incorporation efficiency between 1-nucleotide gapped and primer/template DNA substrates. Also, incorporation efficiency for correct *and* incorrect nucleotides decreased modestly for 5-7 nucleotide gaps, then dropped 160-fold on 10 nucleotide gapped DNA. This is much larger than the difference between 1-nucleotide gapped and primer/template DNA substrates, suggesting an increase in nucleotide incorporation efficiency would occur if the gap were greater than 10 nucleotides. Overall fidelity of hPolβ remained remarkably constant as gap size increased. These results indicate that hPolβ would be less efficient but more accurate than hPolλ in LP-BER (Figure 5).

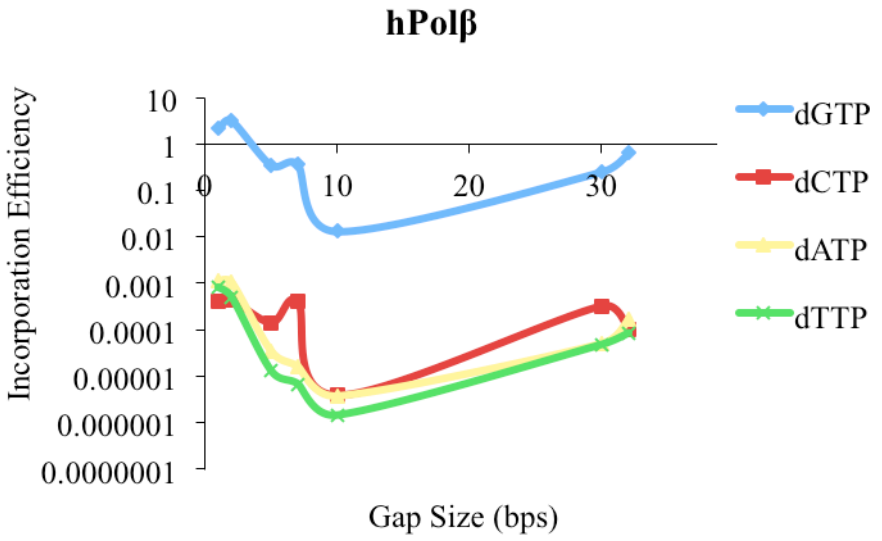

Figure 5. Effect of gap size on the incorporation efficiency of hPolβ. The points at a gap size of "30" indicate incorporation efficiency on primer/template DNA substrate.

The effect of hPolλ's N-terminal domains on its ability to perform gap-filling synthesis: As stated in the Background, hPolλ differs structurally from hPolβ in that it has additional N-terminal BRCT and proline-rich domains. In order to determine the effect of the N-terminal domains on the gap-filling ability of hPolλ, two truncated mutants of hPolλ were created. The first, dPolλ, lacks the BRCT domain. The second, tPolλ, lacks both the BRCT and proline-rich domains (Figure 6).

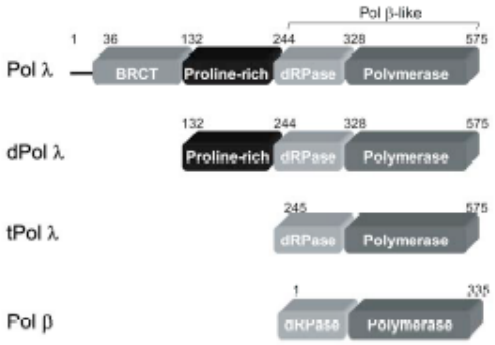

Figure 6: Sequence comparison of hPolβ, hPolλ and mutants of hPolλ.

Single turnover kinetic studies of tPolλ and dPolλ were done on primer/template DNA substrate as well as on DNA substrates containing gaps of 1, 2, 5, 7, and 10 nucleotides. A complete summary of the results from these assays, including calculated k_p, K_D, incorporation efficiency, efficiency ratio, and misincorporation fidelity can be found in Appendix 1, Tables 3 and 5. The following is a summary of the notable results and our observations:

Like hPolλ, both dPolλ and tPolλ displayed a decrease in dGTP incorporation efficiency on primer/template DNA in comparison to 1-nucleotide gapped DNA (28-fold and 6-fold, respectively). Also like hPolλ, dGTP incorporation efficiency for dPolλ and tPolλ stayed relatively constant on gap sizes up to 7 nucleotides and decreased dramatically on 10 nucleotide gapped DNA. However, both truncated versions of hPolλ maintained a higher overall fidelity than hPolλ as gap size increased, indicating that their presence collectively *reduces* the polymerase fidelity of full-length hPolλ by enhancing the polymerase's propensity for misincorporation (Figure 7).

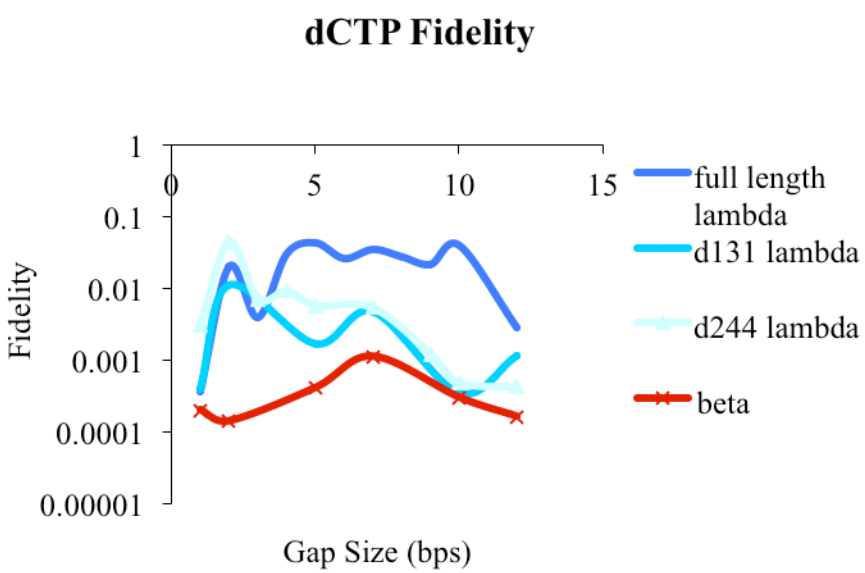

Figure 7. Effect of increasing gap size on propensity of three mutants of hPolλ and hPolβ to misincorporate dCTP. 'Full lambda' denotes hPolλ, 'd131 lambda' denotes dPolλ, 'd244 lambda' denotes tPolλ, and beta denotes hPolβ. Fidelity was calculated using Equation 3, and lower numbers indicate a lower chance of misincorporation AKA a higher overall probability of correct nucleotide incorporation.

A note on sequence dependence: After observing the preference of all four DNA polymerases to misincorporate dCTP, we hypothesized that the preference for dCTP misincorporation was due to the presence of a template dG immediately downstream of the initial template dC. We tested this hypothesis by changing the 42-mer template DNA sequence from 3'-CGG-5' to 3'-CGA-5' and 3'-CAG-5' and performing single-turnover experiments similar to those described previously with hPolλ, tPolλ, dPolλ, and hPolβ. In experiments performed with template 3'-CAG-5', dTTP became the preferred misincorporation. In experiments performed with template 3'-CGA-5', dCTP remained the preferred

misincorporation, suggesting that only the adjacent nucleotide had an impact on misincorporation efficiency. As observed with template 3'-CGG-5' in which dCTP misincorporation efficiency increased with increasing gap size, the misincorporation efficiency of dTTP also increased with increasing gap size, as demonstrated by kinetic parameters obtained on template 47-mer containing 3'-CAT-5' instead of 3'-CGG-5'. The full results of template dependence studies can be found in Appendix 1, Tables 6-9.

Discussion

Though the basic BER pathway is known, the specific enzymes that perform each step are still unclear. For example, six mammalian DNA polymerases have been proposed to perform the gap-filling step of SP-BER and LP-BER, including DNA polymerases beta, delta, epsilon, lambda, iota, and theta[12]. Characterizing the abilities of hPolλ and hPolβ to fill gaps in DNA added to knowledge of their biochemical function and gave insight into how they might function in both SP-BER and LP-BER. Key findings were as follows: 1) 9 nucleotides was the maximum gap size for efficient nucleotide incorporation by hPolλ, 2) as gap size increased from 2-10 nucleotides, fidelity of hPolλ decreased, 3) the N-terminal domains of hPolλ downregulate its fidelity on 2-10 nucleotide gapped DNA, 4) the preferred misincorporation was based on the first downstream template base, 5) the fidelity of hPolβ remained similar as gap size increased, though incorporation efficiency decreased. The following is a more detailed discussion of these key findings:

A structure-function discussion of Polλ: As mentioned, an important observation in our kinetic studies was that the incorporation efficiency of hPolλ remained relatively constant up to a gap size of 9. Crystal structures of hPolλ in complex with 2 nucleotide gapped DNA substrate

give insight into this ability to efficiently incorporate nucleotides; the first downstream template base can be bound in a "scrunching pocket", forming a loop that allows the polymerase to simultaneously maintain contacts with the 3'-hydroxyl, nascent base pair, and 5'-phosphorylated downstream strand[13]. It can be hypothesized that, until a gap size of 9 nucleotides, the loop becomes larger yet can still be accommodated by the polymerase. However, at a gap of 10 nucleotides the loop is too large for contact with the 3'-hydroxyl, nascent base pair, and 5'-phosphorylated downstream strand to all be maintained. This loss of looping ability would therefore account for the dramatic decrease in incorporation efficiency on 10 nucleotide gapped DNA. However, it should be noted that these suppositions are based on the crystal structures of truncated versions of hPolλ; the structure of the full-length version of hPolλ has not yet been solved. This lack of full-length crystal structure also complicates analysis of the structural basis of downregulation of fidelity by hPolλ's N-terminal BRCT and proline-rich domains. Even so, based on the observation that downregulation of fidelity occurred as gap size increased it can be proposed that the N-terminal domains of hPolλ sterically hinder its ability to form large DNA loops that allow simultaneous polymerase interaction with the 3'-hydroxyl, nascent base pair, and 5'-phosphorylated downstream strand.

The ability of hPolλ to 'scrunch' template DNA may also account for the observed misincorporation preference. Our kinetic analyses of sequence dependence indicated that the preferred misincorporation is influenced by the first downstream template base; i.e., downstream template dG made dCTP the preferred misincorporation. This indicates a DNA misalignment, which we hypothesize is due to the same scrunching pocket that allows DNA with gaps of up to 9 nucleotides to be accommodated by hPolλ. In short, the second downstream base may instead occupy the scrunching pocket, stabilizing the misalignment of primer and template (Figure 1,

Appendix 1). This means the initial template base would be skipped, generating frameshift mutations. In accordance with this hypothesis, frameshift mutations *have* been shown to be characteristic of hPolλ[14]. Because we also observed misincorporation preferences for dPolλ and tPolλ, it can be surmised that the N-terminal BRCT and proline-rich domains have minimal influence on stabilization of template misalignment.

Comparison of hPolλ and hPolβ: In the course of the above studies, hPolλ and hPolβ displayed discrete kinetic trends. This agrees with previous observations that, though hPolλ and hPolβ are homologs, they have different enzymatic properties[15,16]. They share an increased incorporation efficiency on 1 nucleotide gapped DNA, probably due to interactions between the polymerase dRPase domain and the 5'-phosphorylated downstream strand. This is evidence of the specialization of hPolλ and hPolβ for gap-filling. However, the impact of a downstream strand was much less pronounced for hPolβ; a 3-fold increase rather than the 33-fold increase observed for hPolλ. Additionally, hPolβ was able to maintain its fidelity but lost incorporation efficiency as gap size, while hPolλ did not. Both enzymes showed a dramatic loss in incorporation efficiency on DNA containing a 10 nucleotide gap, though hPolβ was able to recover if the downstream strand was absent while hPolλ was not. All of this indicates that contacts between the polymerase dRPase domain and 5'-phosphorylated downstream strand are much more critical for the incorporation efficiency of hPolλ than hPolβ, perhaps because the contacts formed stabilize a conformation of hPolλ in which the nascent base pair is well-positioned in the active site[17]. This possibility would also indicate that hPolβ is less dependent on interactions between its dRPase domain and the 5'-phosphorylated downstream strand for optimal positioning of the nascent base pair, and that DNA containing longer gaps actually

hinders this catalytically competent conformation[18]. As there is no structural evidence of how hPolβ accommodates DNA with larger gaps, further interpretation of this possibility cannot yet be made.

The roles of hPolλ and hPolβ in BER: As noted previously, hPolλ and hPolβ were comparably competent at filling 1 nucleotide gapped DNA. This indicates the hPolλ could aptly perform SP-BER. Analyzing the possible involvements of hPolλ and hPolβ in LP-BER solely on our kinetic evidence is somewhat more complicated. Based on maintenance of polymerase fidelity and the cell's goal of genomic integrity, hPolβ is better suited to LP-BER. However, hPolβ loses catalytic efficiency with increasing gap size. hPolλ was the opposite; maintaining catalytic efficiency yet losing fidelity with increasing gap size.

Though there is evidence for hPolβ's involvement in LP-BER[9], I also propose that there is sufficient evidence for the implication of hPolλ in LP-BER. Notably, BER mutational spectra gathered from cell line extracts show an abundance of deletion mutations. As discussed in the context of our sequence dependence, deletion mutations may be indicative of the catalytic presence of hPolλ.

Though hPolλ and hPolβ were the only enzymes examined in this study, the involvement of other DNA polymerases in the gap-filling step of BER cannot be overlooked. It has been hypothesized previously that a combination of DNA polymerases is required for BER, especially LP-BER. The gap-filling activity of hPolβ and hPolλ was proposed to be limited to one nucleotide, either through cooperation with flap endonuclease I which would specifically generate a 1 nucleotide gap[20], or through cooperation with a replicative DNA polymerase which would take control from hPolλ or hPolβ after insertion of the initial nucleotide at the previously

damaged site[21,22]. Though these mechanisms are hypothetical, the combination of this study with those conducted previously cannot exclude either hPolλ or hPolβ as potential players in SP-BER and LP-BER.

Chapter 2: The Mutagenic Spectra of Cyclobutane Thymine Dimer Bypass by Y-family DNA Polymerases

Background

As mentioned in the Introduction, UV light is one of many agents that can damage DNA. The most prevalent result of UV irradiation of DNA is the *cis-syn* cyclobutane thymine dimer (TT dimer, Figure 1). TT dimers stall replicative DNA polymerases, and thus must be processed efficiently for the cell to survive and maintain optimal function. The cell responds to TT dimers in one of three ways. First, dimerization can be directly reversed by a photolyase, which uses a radical mechanism to revert the TT dimer to undamaged, adjacent thymines. Second, the dimer can be processed through the nucleotide excision repair (NER) pathway, in which a section of 25-30 nucleotides around and including the TT dimer are removed and the resulting gap filled. Finally, in cases where DNA replication *is* stalled by an unrepaired TT dimer, the cell must depend on specialized enzymes to bypass the lesion[24]. The Y-family DNA polymerases are among the enzymes that can perform lesion bypass. Though they share nucleotide incorporation activity with replicative DNA polymerases, the Y-family enzymes have much more open active sites. These open active sites allow them to incorporate nucleotides opposite lesions that are not tolerated by the rigid active sites of replicative DNA polymerases[25].

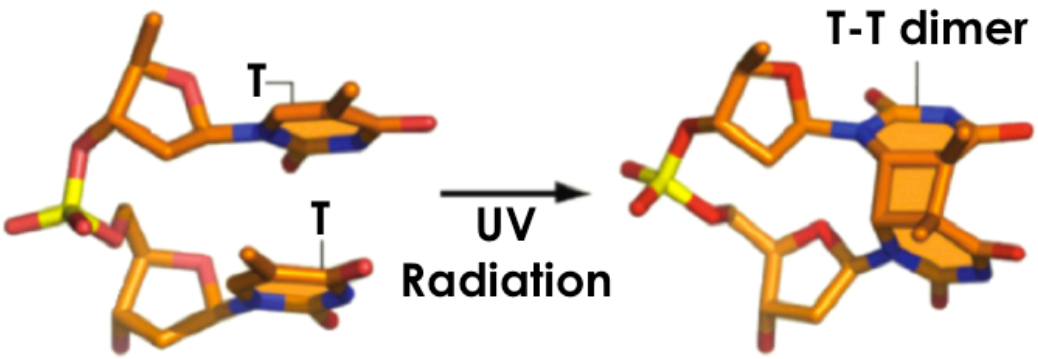

Figure 1. Crystal structure of adjacent undamaged thymines (left) and *cis-syn* cyclobutane thymine dimer (right)[33].

Interestingly, humans do not encode a photolyase and therefore depend on NER and lesion bypass to process TT dimers[26]. Understandably, this makes proper NER and lesion bypass function very important. Xeroderma pigmentosum is visible proof of this importance. XP is characterized by extreme sensitivity to sunlight and increased incidence of skin cancer. Furthermore, it is caused by defects in NER or lesion bypass enzymes. The variant form (XPV) is specifically due to mutation of the gene encoding human DNA polymerase eta (hPolη), a member of the Y-family of DNA polymerases[27]. Therefore, though lesion bypass is the last resort of the DNA damage response, loss of the ability to bypass UV-induced photoproducts is damaging enough to have an observable phenotype.

As can be expected, hPolη is the prime candidate to perform TT dimer bypass *in vivo*. *In vitro* kinetic studies support this claim, demonstrating that hPolη preferentially bypasses TT dimers in an error-free manner. In fact, hPolη incorporates nucleotides *more* efficiently in the vicinity of a *cis-syn* cyclobutane thymine dimer[28], which is especially surprising due to the 20-

30˚ distortion induced by a TT dimer[29]. Recent structural studies propose an explanation for the fidelity and efficiency of TT dimer bypass by hPolη. Fidelity is maintained because hPolη stabilizes DNA containing a TT dimer into the normal B-form, promoting Watson-Crick base pairing. This, along with the ability of hPolη to accommodate both thymines of the dimer in its active site, also increases nucleotide incorporation efficiency[30].

Though hPolη is likely to bypass TT dimers *in vivo*, it is not the only member of the Y-family of DNA polymerases (Figure 2). Humans encode 3 other Y-family members; human DNA polymerase kappa (hPolκ), human DNA polymerase iota (hPolι), and human Rev1 (hRev1). As mentioned before, they all have open active sites that allow them to perform lesion bypass. However, this open-ness often makes lesion bypass error-prone due to loss of the steric requirement that normally promotes Watson-Crick base pairing. The Y-family enzymes are also distributive, meaning they only incorporate a few nucleotides in a single DNA-binding event.

Previous studies indicate specialized cellular roles for each Y-family member. hPolκ is thought to bypass bulky minor-groove adducts and to extend from the lesion bypass products of other DNA polymerases[35]. hPolι has been shown *in vitro* to bypass a variety of lesions, including TT dimers and 6-4 TT photoproducts[32]. Finally, hRev1 is primarily a dCTP transferase, using one of its own amino acids as a template rather than using DNA[37]. hRev1 is also thought to play a role in recruitment and managing of the lesion bypass process, possessing domains that enable it to interact with the other Y-family members[25].

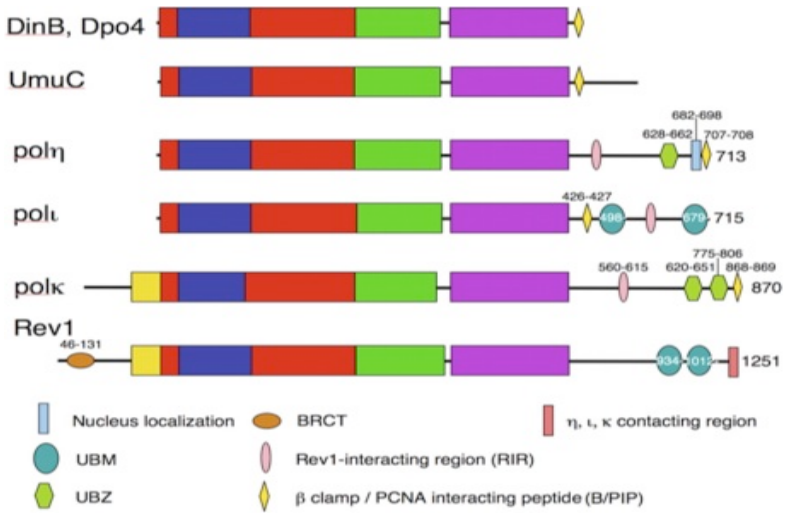

Figure 2. Sequence alignment of several Y-family DNA polymerases. Palm domain is in red, finger domain in blue, thumb domain in green, little finger domain in purple, and n-digit in yellow. All interaction regions are otherwise identified.

Though hPolη and hPolι have been proven to bypass TT dimers[28,31,32], the response of the other Y-family DNA polymerases to TT dimers is less well known. Also unclear is how the lesion bypass response changes in XPV patients. Sequence data indicate an unusually high frequency of UV-induced mutation, the majority of which are transversions. It has been hypothesized that this characteristic mutation spectra is indicative of a DNA polymerase performing error-prone lesion bypass[27]. With this information, the goals of this study were 1) to confirm TT dimer bypass ability by hPolη, hPolι, and the model Y-family member from *Sulfolobus solfataricus,* DNA Polymerase IV[29] (Dpo4), 2) to test the TT dimer bypass ability of hPolκ and hRev1, and 3) to characterize the mutagenic profile of lesion bypass by the human Y-family DNA polymerases and Dpo4.

Methods

Materials: In addition to the reagents listed in Chapter 1, the following were purchased: synthetic deoxyribonucleotide 25-mer, 31-mer, 51-mer, 77-mer control, primer 17-mer, and reverse PCR primer 21-mer from Integrated DNA Technologies, T4 DNA ligase from New England BioLabs, T4 polynucleotide kinase from New England BioLabs, *Taq* DNA polymerase from Fermentas, and TOPO TA Cloning Kit from Invitrogen. A synthetic 21-mer containing a site-specific cyclobutane thymine dimer (21-mer TT) was acquired from Dr. John-Stephen Taylor at Washington University in St. Louis. Human DNA polymerase kappa (hPolκ), human DNA polymerase eta (hPolη), human DNA polymerase iota (hPolι), human Rev1 (hRev1), and *Sulfolobus solfataricus* DNA Polymerase IV (Dpo4) were purified as described previously[25]/

Ligation of 77-mer containing a site-specific cyclobutane thymine dimer adduct: Synthetic deoxyribonucleotides were purified using polyacrylamide gel electrophoresis. Purification was shared between myself and other members of the Suo lab. Concentration of the purified deoxyribonucleotides was determined using UV spectroscopy at 260 nM. The 31-mer and 21-mer TT were 5'-phosphorylated by T4 polynucleotide kinase in the presence of 5 mM ATP. The 5'-phosphorylated 21-mer TT and 31mer were mixed with the 51-mer and 25-mer at a 1.0:1.0:1.0:1.0 molar ratio. This mixture was heated to 70˚C for 8 minutes and then cooled slowly to promote annealing. T4 DNA ligase buffer and T4 DNA ligase were added to this mixture according to the manufacturer's protocol. Ligation occurred over a 48 hour period at 16˚C, with addition of fresh T4 DNA ligase at 24 hours. Successfully ligated 77-mer containing a site-specific cyclobutane thymine dimer adduct (77-mer TT) was separated from the rest of the

reaction mixture using 10% acrylamide 8M urea gel electrophoresis and purified as described in Chapter 1. I personally performed ligation of the 77-mer TT.

Annealing of 17/77-mer control and TT: To generate a primer/template substrate for the running start and short oligonucleotide sequencing assays, 17-mer was mixed with either 77-mer control or 77-mer TT at a 1.2:1.0 molar ratio. The mixture was heated to 95˚C for 5 minutes in the case of the 77-mer control and to 70˚C for 8 minutes in the case of the 77-mer TT, then cooled slowly to room temperature. For running start assays, a fraction of the 17-mer was 5'-[^{32}P]-radiolabeled as described in Chapter 1.

Reaction Buffer: Reactions were performed in optimized buffer "R"; 50 mM HEPES pH 7.5 at 37˚C, 5 mM $MgCl_2$, 50 mM NaCL, 0.1 mM EDTA, 5 mM dithiothreitol, 10% glycerol, and 0.1 mg/mL bovine serum albumin. As before, these concentrations are indicative of solution concentrations after mixing of all components

Running Start Assays: The running start assays were performed by mixing pre-incubated 17/77-mer control or TT (100 nM) and Y-family DNA polymerase (100 nM) in buffer "R'" with a solution containing all four dNTPs (200 μM each). At various time points an aliquot was removed from the reaction and quenched in EDTA to a final [EDTA] of 0.37 M. Reaction products were separated using 17% acrylamide 8M urea gel electrophoresis and visualized using a Typhoon TRIO (GE Healthcare). The reactions for hPolι and hRev1 were performed personally by hand, and the reactions for hPolη, hPolκ, and Dpo4 by Shanen Sherrer using rapid chemical-quench as described in Chapter 1.

Short Oligonucleotide Sequencing Assays (SOSAs):

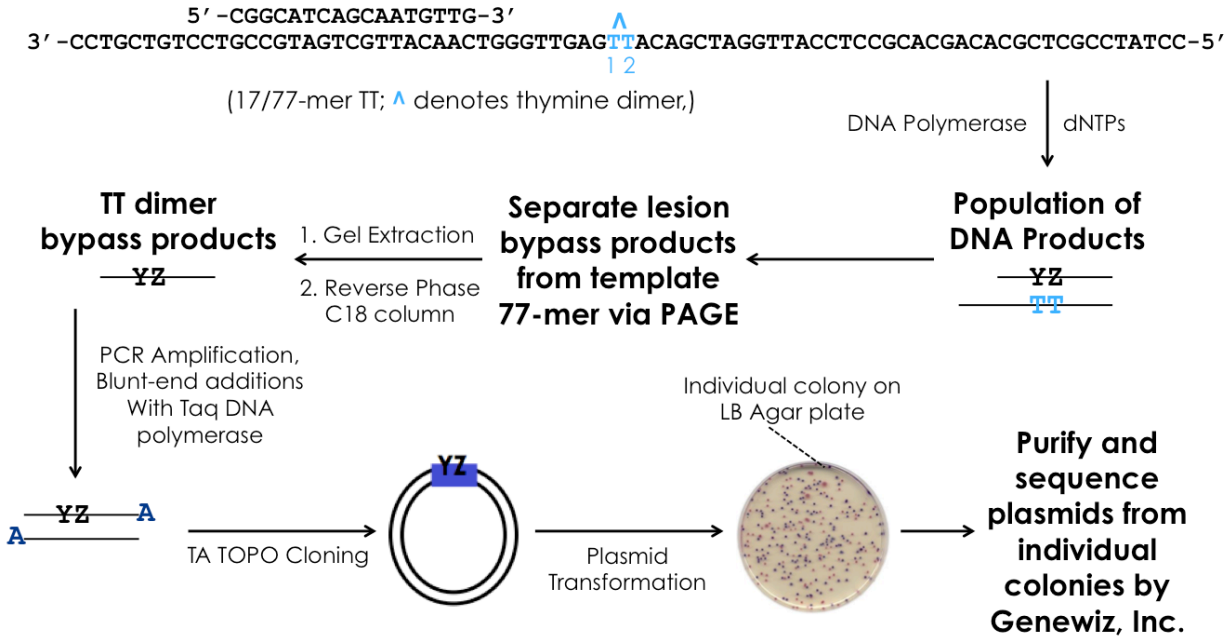

Figure 3. Short Oligonucleotide Sequencing Assay Scheme

SOSAs were performed by mixing pre-incubated 17/77-mer control or TT (120 nM) and Y-family DNA polymerase (30 nM) in buffer "R" with a solution containing all four dNTPs (200 μM). SOSAs were performed for all four human Y-family DNA polymerases and Dpo4; all on both 77-mer control and 77-mer TT. Each reaction proceeded for a time period optimized to maximize the amount of full-length (66-mer) product while minimizing any DNA degradation. To terminate the reaction, the mixture was subjected to 3 freeze-thaw cycles (-196˚C to 95˚C). Full-length 66-mer product was separated from template 77-mer and incompletely replicated deoxyribonucleotides using 10% acrylamide 8M urea gel electrophoresis. The isolated products were amplified using polymerase chain reaction (PCR), aided by *Taq* DNA polymerase, 17-mer forward PCR primer, and 21-mer reverse PCR primer. These primers were designed to create a sequencing 'window' of 28 bases, including 10 bases prior to the cyclobutane thymine dimer and

16 bases after cyclobutane thymine dimer encounter. The population of amplified DNA products were ligated into a pCR4-TOPO vector using a TOPO TA cloning kit (Invitrogen) and transformed into TOP10 *E.coli* (Invitrogen) according to the manufacturer's directions. Individual colonies, each potentially indicative of a different full-length product, were picked and their plasmids sequenced (Genewiz, Inc). SOSA duties were shared between myself and Shanen Sherrer.

Results

Running start assays: While performing running start assays of human Y-family DNA polymerase and Dpo4 bypass of cyclobutane thymine dimers, we had two primary goals. First, we intended to confirm that TT dimer bypass is possible for hPolη, hPolι, and Dpo4. The abilities of Dpo4 and hPolη to bypass TT dimers have been studied previously via running start assays[31], though not under consistent reaction conditions or the conditions used in our short oligonucleotide sequencing assays. The ability of hPolι to incorporate nucleotides opposite a TT dimer was previously observed by steady state kinetic assays[32], but not running start assays. It is instructive to perform running start assays in addition to kinetic assays of nucleotide incorporation at the lesion in order to observe polymerase behavior before, after, *and* at the lesion. The second aim of our running start assays was to test the ability of hPolκ and hRev1 to perform TT dimer bypass, which is largely unstudied.

We observed that all DNA polymerases studied were able to bypass a cyclobutane thymine dimer to varying degrees. This ability was indicated by the presence of product past the site of the lesion on 17/77-mer primer/template DNA containing a site-specific TT dimer. For

each running start assay performed on 17/77mer-TT DNA substrate, a similar running assay was performed on 17/77-mer control DNA substrate for comparison.

DNA substrates for running start assays and SOSAs
17/77-mer control
5′-CGGCATCAGCAATGTTG-3′ 3′-CCTGCTGTCCTGCCGTAGTCGTTACAACTGGGTTGAGTTACAGCTAGGTTACCTCCGCACGACACGCTCGCCTATCC-5′
17/77-mer TT
5′-CGGCATCAGCAATGTTG-3′ 3′-CCTGCTGTCCTGCCGTAGTCGTTACAACTGGGTTGAG^TTACAGCTAGGTTACCTCCGCACGACACGCTCGCCTATCC-5′

Table 1. Annealed 17/77-mers for running start assays and SOSAs. The position of the lesion is highlighted in blue with the dimer indicated by a ^.

In general, we looked for pause sites on both control and damaged DNA substrates, indicative of polymerase stalling. The following is a brief relation of the pausing patterns of each enzyme:

i. hPolη: On control DNA, hPolη exhibited no significant pausing. On damaged DNA, several pause sites were observed. Several pause sites were areas of sequence redundancy (positions 20, 21, 24). hPolη also stalled at position 27, or upon insertion opposite T2 of the TT dimer. No further pausing was observed (Appendix 2, Figure 1).

ii. hPolκ: On control DNA, hPolκ exhibited no significant pausing. On damaged DNA, several pause sites were observed. As with hPolη, hPolκ stalled at areas of sequence redundancy (positions 20 and 22). The running start assay for hPolκ also displayed product accumulation at positions 26 and 27, indicating stalling upon insertion opposite both dTs of the TT dimer. No further pausing was observed (Appendix 2, Figure 2).

iii. hPolι: Pausing was observed in similar locations on both control and damaged DNA. Speciifcally, strong pausing occurred in areas of sequence redundancy (positions 18, 21, 22). Cyclic pausing was also observed downstream of the site of the TT dimer at positions 32, 34, 37, and ~42. The difference in pausing observed between control and damaged DNA is solely around the site of the TT dimer, specifically in the amplified product accumulation at positions 26 and 28 that is indicative of stalling upon insertion opposite the first dT of the TT dimer and upon extension from the TT dimer (Appendix 2, Figure 3).

iv. hRev1: Pausing was observed on both the control and damaged DNA templates. As with hPolι, these were often areas of sequence redundancy (position 22). There was also significant pausing at positions 24, 25, 26, and slightly at 27 on the control substrate and positions 25, 26, 27, and 28 on the damaged substrate. On the damaged substrate this indicates pausing upon insertion opposite each dT of the TT dimer, extension from the lesion, and immediately prior to lesion encounter. On the control substrate this indicates pausing opposite template purines dA and dG and opposite both dTs of a doublet dT (Appendix 2, Figure 4).

v. Dpo4: On control DNA, Dpo4 exhibited no significant pausing. On damaged DNA, several pause sites were observed. As with the other DNA polymerases, sequence redundancy caused polymerase stalling (positions 18, 20). Dpo4 also stalled upon nucleotide incorporation opposite T1 of the TT dimer (Appendix 2, Figure 5).

The running start assays also allowed us to extract quantitative data about the relative TT dimer bypass efficiencies of the human Y-family DNA polymerases and Dpo4. Specifically, we calculated %bypass of each dT of the TT dimer and % bypass of the complete lesion at each time

point using Equation 4. By plotting the % bypass over time, we estimated a t_{50} of T1 bypass, T2 bypass, and whole lesion bypass for each enzyme studied.

% bypass = (bypass events/encounter events) x 100% Equation 4

Note: T1 bypass events were found by summing the concentration of all intermediate and full length products of size ≥27 base pairs. T2 bypass and whole lesion bypass events encompassed all bands ≥28 base pairs. T1 and whole lesion encounter events encompassed all bands ≥26 base pairs, T2 encounter events encompassed all bands ≥27 base pairs.

Based on t_{50} bypass values, hPolη was the most efficient at bypass of T1, T2, and the whole lesion, followed by Dpo4, hPolκ, hPolι, and hRev1 (Table 2). Though hRev1 displayed a t_{50} bypass for both T1 and T2, it did not bypass 50% of the whole TT dimer in the time surveyed (4 hours). This is possible because, for bypass of T1 and T2, only encounter events for that particular nucleotide were accounted for. At each time point there were fewer encounter events for T2 than T1, especially due to polymerase stalling at T1. Additionally, t_{50} of whole lesion bypass takes into account the encounter events for T1 and the bypass events for T2, and therefore is a longer estimated time. The same reasoning can be carried over to all Y-family DNA polymerases studied, though only hRev1 did not reach a t_{50} of whole lesion bypass.

Enzyme	t_{50} T1 bypass (s)	t_{50} T2 bypass (s)	t_{50} lesion bypass (s)
hPolη	0.77	0.79	16.79
hPolκ	14.6	33.5	304
hPolι	70	297	1586
hRev1	5229	7789	not observed
Dpo4	0.8	23.5	52.1

Table 2. A summary of estimated t_{50} of T1, T2, and whole lesion bypass by Y-family DNA polymerases.

Short oligonucleotide sequencing assays: As stated previously, our goal in performing SOSAs was to observe the mutagenic spectra of TT dimer lesion bypass. Specifically, we

observed deletion, substitution, and insertion mutations within a 28 nucleotide sequencing window that encompasses, pre-lesion, lesion, and post-lesion events. This method generates data that is complementary to kinetic studies though broader in scope. It should be noted that these assays are still in progress, thus the data presented herein is preliminary. For each enzyme, SOSAs were performed on a 77-mer TT DNA substrate in order to observe mutagenic preference opposite the lesion. SOSAs were also performed on a 77-mer control DNA substrate so that the effect of the TT dimer on upstream and downstream incorporations could be evaluated. The following is a summary of the results for each enzyme:

i. hPolη: 11 colonies have been sequenced for control DNA and data collection is still in process for damaged DNA. Control sequences indicate a random spectrum of mutations with no notable increase in mutagenicity at any spot on the template (Appendix 2, Figure 6).

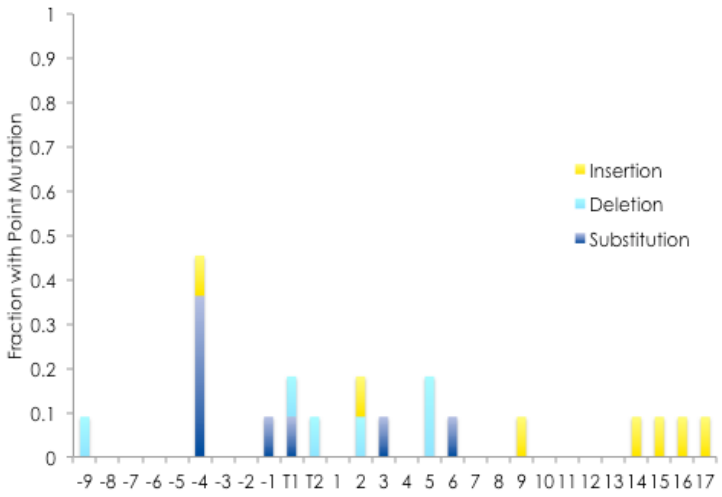

Figure 4. The mutagenic spectra of polymerization by hPolη on 77-mer control DNA. The relevant template sequence is denoted below the chart.

ii. hPolκ: 25 colonies have been sequenced for control DNA and 14 for damaged DNA. At the TT dimer, hPolκ bypassed accurately, made double base deletions, or made double base substitutions. Accurate bypass accounted for 21.4% of sequences, double base deletions for 35.7%, and double base substitutions for 42.9%. Substitutions observed at the lesion were all insertion of T opposite T1 and insertion of either G or C opposite T2. Random mutations were observed upstream and downstream of the lesion, with a notable increase 4 and 5 bases downstream of the lesion (positions 32 and 33). A random spectrum of mutation was also observed on control DNA, with no particular increase in mutagenicity at any spot on the template (Appendix 2, Figures 7 and 8).

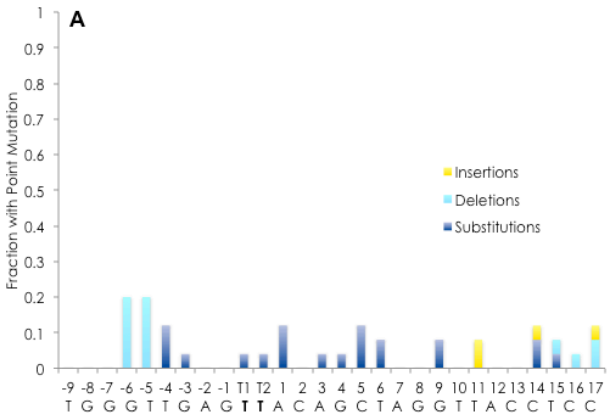

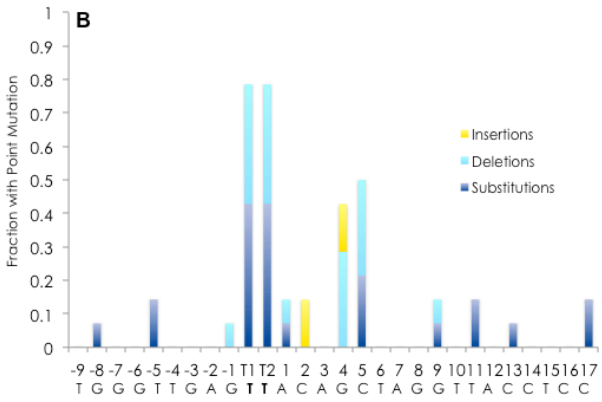

Figure 5. The mutagenic spectra of polymerization by hPolκ on A. 77-mer control DNA, B. 77-mer TT DNA. The relevant template sequences are denoted below the chart, as well as position from the lesion.

iii. hPolι: 6 colonies were sequenced for control DNA and 21 colonies were sequenced for damaged DNA. At the TT dimer, hPolι made a double base deletion or a single base substitution. Double base deletions accounted for 95.2% of sequences, and single base substitutions (T opposite T1) accounted for 4.8% of sequences. Random mutations were observed both upstream and downstream of the lesion. Interestingly, the mutagenic events were roughly cyclic, i.e., there was an increase in mutations approximately every 4-5 nucleotides before and after the TT dimer. A random spectrum of mutations was observed for control 77-mer, with the only notable increases being at positions 27, 28, and 44 of the DNA template (Appendix 2, Figures 9 and 10).

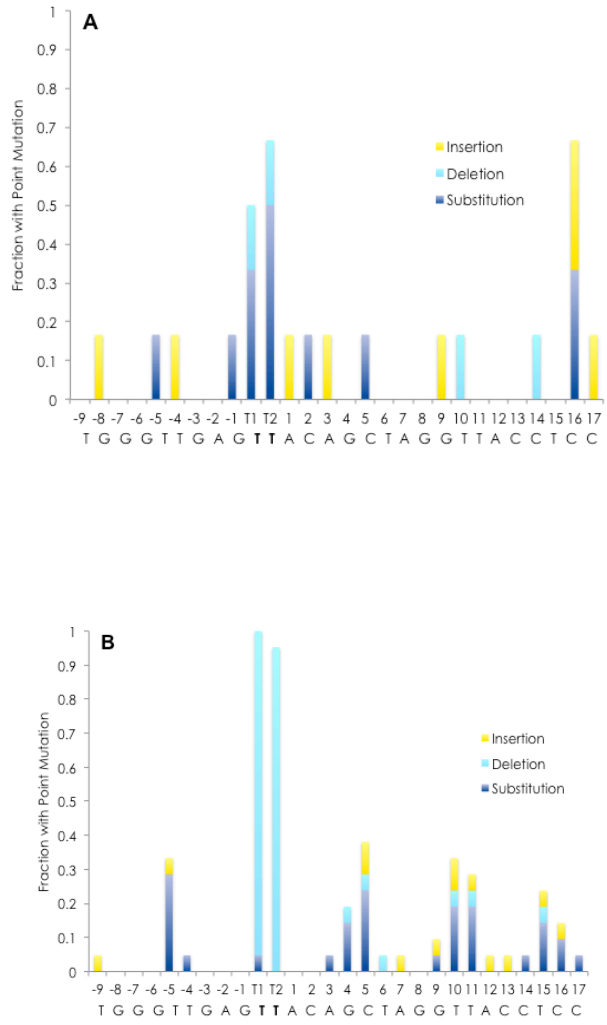

Figure 6. The mutagenic spectra of polymerization by hPolι on A. 77-mer control DNA, B. 77-mer TT DNA. The relevant template sequences are denoted below the chart, as well as the position from the lesion.

iv. hRev1: Data collection is still in process for hRev1.

v. Dpo4: 65 colonies were sequenced for control DNA and 28 colonies were sequenced for damaged DNA. At the TT dimer, Dpo4 bypassed accurately, made a double base deletion, made a single base substitution, or performed a combination substitution-deletion. Accurate bypass accounts for 32.1% of sequences, double base deletion for 46.4% of sequences, single

base substitution for 17.9% of sequences, and combination substitution-deletion for 3.6% of sequences. Notably, all single base substitutions were incorporation of C opposite T2 of the TT dimer. Remarkably few mutations were observed on 77-mer control DNA template; only 4 substitutions out of 65 sequences (Appendix 2, Figures 11 and 12).

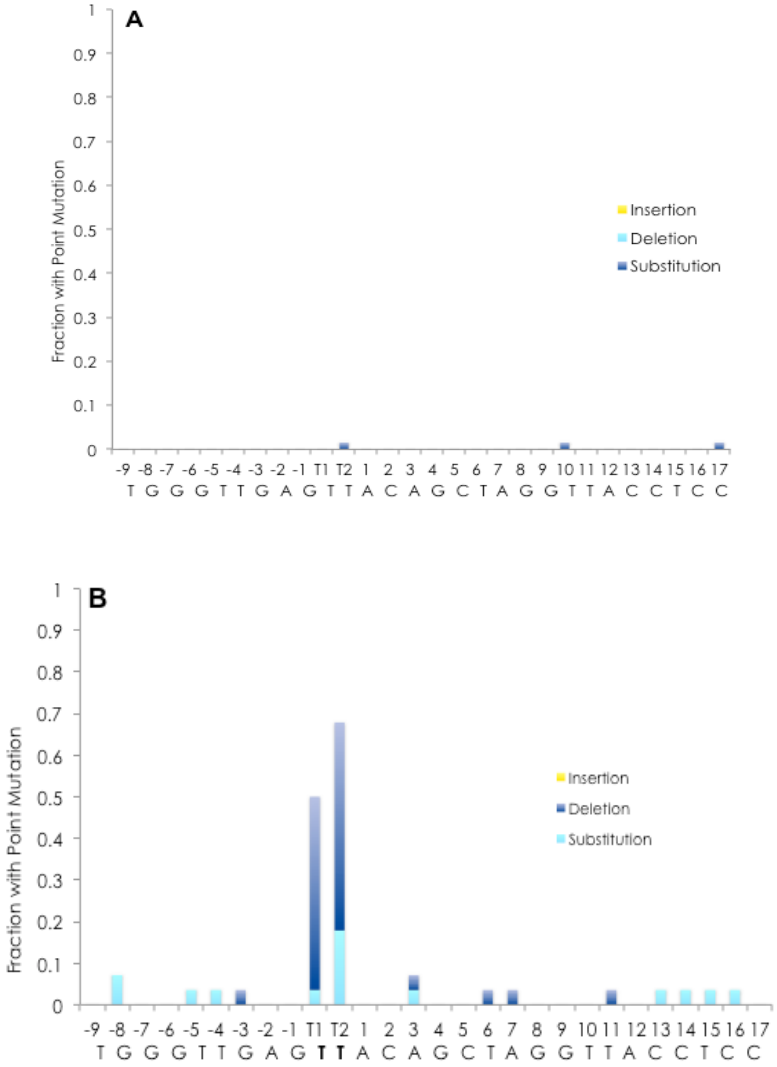

Figure 7. The mutagenic spectra of polymerization by Dpo4 on A. 77-mer control DNA, B. 77-mer TT DNA. The relevant template sequences are denoted below the chart.

After initial sequence analysis, we also found the total error frequency of each Y-family DNA polymerase on both control and damaged templates using Equation 5 (Table 3).

Enzyme	Total Error Frequency (77-mer control)	Total Error Frequency (77-mer TT)	Total Error Frequency except TT dimer site (77-mer TT)
hPolκ	5.6×10^{-2}	1.5×10^{-1}	1.0×10^{-1}
hPolη	8.4×10^{-2}	--	--
hPolι	1.4×10^{-1}	1.7×10^{-1}	1.0×10^{-1}
hRev1	--	--	--
Dpo4	2×10^{-3}	6.1×10^{-2}	2×10^{-2}

Table 3. The total error frequencies on control and damaged DNA, calculated using Equation 5.

Total error frequency = total # mutations / # bases sequenced Equation 5

In summary, efficiency of TT dimer bypass by the Y-family DNA polymerases studied is as follows: hPolη > Dpo4 > hPolκ > hPolι > hRev1. Dpo4 was least error prone on control DNA, followed by hPolκ, hPolη, and hPolι. Thus far, Dpo4 is also least error prone on damaged DNA, followed by hPolκ and hPolι. hPolη remains to be sequenced for 77-mer TT DNA substrate. Polymerase stalling was observed at both the TT dimer and in areas of DNA redundancy (triplet dG, doublet dT) for all Y-family DNA polymerases studied. DNA redundancy has been observed to cause polymerase stalling in other experiments performed in our lab, and did not correlate with areas of increased error.

Discussion

Cyclobutane thymine dimers are the most common UV-induced DNA lesions. They are problematic because they present a strong block to replicative DNA polymerases and also promote mutation and cancer formation. In humans, lesion bypass is an important process by which cyclobutane thymine dimers (TT dimers) are tolerated. The Y-family of DNA polymerases is specialized for lesion bypass and, in humans, the Y-family DNA polymerase eta (hPolη) has been strongly implicated in TT dimer bypass[24]. In fact, the disease xeroderma pigmentosum variant (XPV), which is characterized by increased incidence of UV-induced skin cancer, is caused by mutations in the gene encoding hPolη. XPV cell lines indicate a characteristic spectrum of transversion mutations, which may be due to changes in the lesion bypass response in the absence of functional hPolη[27]. This study profiles bypass of a TT dimer by all human Y-family DNA polymerases as well as the model Y-family member from *Sulfolobus solfataricus,* DNA Polymerase IV (Dpo4). We employed running start assays and short oligonucleotide sequencing assays for a thorough characterization of the efficiency and mutagenicity of lesion bypass by each DNA polymerase. In accordance with previous studies of the Y-family DNA polymerases, our results suggest that though the Y-family members share lesion bypass ability, they utilize different mechanisms to process DNA lesions[25]. Below, I will discuss our current results in light of previous studies of TT dimer bypass and in light of current mechanistic and structural knowledge of each enzyme.

i. hPolη: As mentioned previously, there is strong support for the theory that hPolη is the major DNA polymerase responsible for error-free TT dimer bypass *in vivo*. The recently published crystal structure of hPolη in complex with DNA containing a TT dimer and incoming

dAMPNPP gives insight into the molecular basis of hPolη's TT dimer bypass ability. hPolη effectively stabilizes both thymines of the dimer in a structure akin to that of undamaged DNA by holding both in its active site at once. This allows for normal Watson-Crick base pairing and relatively error-free lesion bypass[31]. The specialization of hPolη for TT dimer bypass is further indicated by its lowered error frequency on damaged DNA, indicating that a TT dimer may be a better substrate for hPolη than two undamaged thymines[28].

It is interesting that, though hPolη can accommodate both thymines of a TT dimer in its active site at once, nucleotide incorporation efficiency at both thymines is not equal. We observed slight stalling upon incorporation opposite T1 of the lesion, but much more pronounced stalling upon incorporation opposite T2. Fortunately, the ternary crystal structure of yeast DNA polymerase eta (yPolη) may explain this phenomenon. In structures comparing damaged and undamaged DNA, T1 was in almost identical positions. In contrast, T2 shifted subtly in reference to nearby amino acid side chains. Though subtle, this shift was proposed by the authors to account for slight stalling with no observed change in error frequency[33]. We observed slight stalling, but change in error frequency remains to be confirmed by our sequencing data. So far, sequencing data from control DNA substrate indicate a total error frequency of 8.4×10^{-2}, which is in accord with previous studies of the error frequency of hPolη on undamaged DNA. Based on previous studies of hPolη, we expect the total error frequency to be *lower* in the vicinity of the lesion than in the corresponding area of control DNA.

ii. hPolκ: hPolκ is primarily implicated in bypass of bulky minor groove adducts and in extension from DNA lesions[4]. We found that hPolκ was capable of TT dimer bypass, with polymerase efficiency and fidelity second only to hPolη amongst the human Y-family DNA

polymerases. Previous studies indicate that it has a higher fidelity than that of hPolη, usually 10^{-3}-10^{-4} on undamaged DNA. We observed a total error frequency of 5.6×10^{-2}, which is 56- to 560-fold higher than the previous calculations[34]. This discrepancy can be neatly resolved by the ability of hPolκ to extend mismatched primer termini 10-100x more efficiently than matched primer termini. This would lead to mutations being extended more frequently and therefore more frequently observed in our full-length products.

The propensity to extend mismatches may also be critical to the mechanism by which hPolκ was able to perform TT dimer bypass. Only 22% of the sequences collected were results of accurate lesion bypass; the other 78% were the result of hPolκ extending mismatched primer termini due to substitution or deletion mutations. Unfortunately, hPolκ has not been extensively studied in terms of TT dimer bypass, so its exact mechanism of lesion accommodation and nucleotide incorporation is unclear.

As the Y-family DNA polymerase with the highest fidelity, hPolκ also has the most restrictive active site. The running start assay indicates pausing upon incorporation opposite both thymines of the dimer, indicating that hPolκ may only able to hold one template base in its active site at once. Pausing is much stronger upon incorporation of the first dT. This can be explained by the only other study of hPolκ's TT dimer bypass activity; a recent crystal structure of hPolκ incorporating dATP opposite T2 of the lesion. hPolκ is able to hold T2 in the same positioning as an undamaged dT. The authors did not crystallize nucleotide incorporation opposite T1, but theorized that the active site of hPolκ is too restrictive to easily accommodate T1[35]. If true, these hypotheses would explain the pausing pattern observed in our running start assay.

There are two main hypotheses regarding the role of hPolκ in TT dimer bypass. The first is that it is not involved at all. The cornerstone of this hypothesis is that hPolη is known to accommodate both bases of the TT dimer in its active site and to incorporate nucleotides opposite the lesion efficiently and correctly[28]. The binding affinity of hPolη drops 3-4 nucleotides after the lesion, promoting dissociation from DNA and facilitating the switch back to a replicative DNA polymerase. Therefore, a specialized polymerase to extend from the lesion would not be needed. The second hypothesis made by Vasquez-del Carpio et al. is that hPolη only inserts dATP opposite T1 of the dimer, leaving hPolκ to incorporate dATP opposite T2 of the lesion and then extend from the lesion[35]. Our study indicates some pausing by hPolη after incorporation opposite T1, indicating that hPolκ could be involved. In addition, hPolη and hPolκ are both distributive and could feasibly compete for nucleotide incorporation.

iii. hPolι: In this study, we observed that hPolι is able to bypass TT dimers with low bypass efficiency as well as a high rate of polymerase error. The calculated total error frequency of 1.4×10^{-1} on undamaged DNA is in accordance with previous studies of hPolι and likely due to its unusual method of base pairing that varies with template base. For example, though hPolι prefers to form correct Watson-Crick base pairs opposite template dA, it prefers to form wobble pairs opposite template dT. This leads to slight preference of dGTP incorporation over dATP incorporation[36]. We did not observe that extreme of a preference in our mutagenic spectra, though it should be noted that 36% of mutations opposite template dT were the insertion or substitution of dGTP.

Previous steady state kinetic studies indicate a complex mechanism of TT dimer bypass for hPolι. It was observed that hPolι prefers to incorporate dT opposite T1 of the lesion, with

secondary preference for dA incorporation. After incorporation opposite T1, dA is extended more easily, and the most common nucleotide to be inserted opposite T2 is dGTP. However, they then observe that AG is not easily extended from[32]. Interestingly, this could account for the heavy pausing upon extension from the TT dimer observed in our running start assay. It could also explain why the sequences of TT dimer bypass products collected displayed mostly deletions at the site of the lesion, as the previous GC base pair may be more easily extended. Interestingly, the strong pausing and complex interplay of incorporation and extension ability exhibited by hPolι suggests that it could be aided in the cell by a polymerase such as hPolκ, which preferentially extends from mismatched primer termini.

Though hPolι has a low bypass efficiency and overall fidelity, it is currently the prime candidate to perform photoproduct lesion bypass in the absence of functional hPolη. The reasons for this hypothesis are as follows: 1) XPV patients exhibit 10% of normal lesion bypass activity[32], 2) XPV cell line sequences indicate a high rate of dT to dC transversions[27], and 3) hPolι is a paralog of hPolη and therefore may be recruited similarly[32]. Our results are in accord with this hypothesis. The loss of bypass ability can be accounted for by the low catalytic and TT dimer bypass efficiency of hPolι, and the dT to dC transversions can be accounted for by the preference of hPolι to insert dGTP opposite dT, which would lead to a dC in place of dT upon the next round of DNA replication.

iv. hRev1: Though hRev1 is in the Y-family of DNA polymerases, it is technically a dCMP transferase. Instead of determining the incoming nucleotide using a template base, hRev1 uses one of its arginine side chains to pair with an incoming dCTP. Due to this extreme selection bias, it preferentially incorporates dCTP opposite dG, dA, dC, and dT. Therefore, it has been

previously proposed that hRev1's lesion bypass ability is tightly limited to dG adducts[37]. Though we had the surprising result that hRev1 had marginal TT dimer bypass ability, it did not reach a t_{50} bypass in our running start assay. It was also notably inefficient at replicating control DNA, indicative of a low overall incorporation efficiency. Therefore, we believe it is not catalytically involved in TT dimer bypass under normal or hPolη-deficient conditions. Due to extremely low polymerization efficiency and known dCMP transferase activity, we may not sequence hRev1 bypass products. With our method, the sequences collected would likely be results of extreme selection bias.

Though its catalytic activity is limited, hRev1 is still thought to have an important role in lesion bypass. As alluded to in the Background, hRev1 is thought to mediate polymerase switching during lesion bypass. This proposal is due to the ability to interact with proliferating cell nuclear antigen (PCNA), ubiquitinated proteins, and human DNA polymerases eta, kappa, iota, and zeta[38]. In short, hRev1 has a unique role in the cell that deserves further study, but it is not catalytically relevant when studying TT dimer bypass.

v. Dpo4: The archaeon from which Dpo4 originates, *Sulfolobus solfataricus*, is a hyperthermophile. In this extreme environment, the DNA of *S. solfataricus* faces a high level of stress. Thus far, Dpo4 is the only DNA polymerase isolated from this extremophile capable of lesion bypass. This implies that Dpo4 must be proficient at bypassing a wide variety of DNA lesions in an error-free manner in order for *S. solfataricus* to maintain genome integrity and proper cellular functions. Indeed, Dpo4 was efficient at TT dimer bypass and displayed a relatively low rate of mutation on both control and damaged DNA. Its total error frequency on undamaged DNA was 2×10^{-3}, which is in accord with the calculated fidelity of Dpo4 from kinetic studies. The total error frequency rose to 6.1×10^{-2} on damaged DNA, though this is still

lower than the total error frequency on damaged DNA of any human Y-family DNA polymerases.

A heavy pause before nucleotide incorporation opposite the first dT of the TT dimer indicated polymerase stalling. Based on previous steady state kinetic studies of Dpo4, we hypothesize that this is due to the inability of the enzyme to "flip out" T2 of the lesion as it brings T1 into its active site as it would do during normal nucleotide incorporation[31]. We hypothesize that this stalling is due to a slow accommodation step in which Dpo4 brings *both* thymines of the dimer into its active site. This hypothesis is in accordance with the ternary crystal structure of Dpo4, DNA containing a TT dimer, and incoming ddADP, in which Dpo4 did indeed accommodate both thymines in its active site at once[39]. Intriguingly, we observed that this strong pausing point did not correlate with an increase in polymerase error or lowered incorporation efficiency at T1 of the TT dimer. Instead, incorporation occurred with similar fidelity and efficiency at both dTs of the TT dimer. This is in accord with previous steady state kinetic studies of incorporation at the lesion[31].

It should be noted that the aforementioned steady state kinetic and crystallographic studies disagree on their interpretations of the mechanism by which Dpo4 bypasses a TT dimer – not only in the details mentioned above but also in the absence or presence of a translocation step and in the type of base pairing (Watson-Crick or Hoogsteen) used to incorporate dATP opposite the lesion. Our investigation supports a slow TT dimer accommodation step in which both thymines are brought into the active site of Dpo4, followed by relatively equal efficiency and fidelity of nucleotide incorporation opposite the lesion. However, further clarification of Dpo4's TT dimer bypass mechanism is necessary to resolve the dispute between steady state kinetic and structural studies.

vi. The effect of DNA structure on DNA polymerase fidelity: As mentioned above, the presence of a TT dimer had both local and global effects on polymerization fidelity. Local effects were noticed upon insertion opposite both dTs of the TT dimer and upon the subsequent extension step from the TT dimer. Global effects were noticed on an overall increase in error frequency on the damaged DNA substrate. The crystal structure of cyclobutane thymine dimer-containing DNA may explain this increase in total error frequency; the presence of a TT dimer bends the helix by 30˚ towards the major groove and unwinds the helix by 9°[29]. The mutagenic spectra of TT dimer bypass by hPolκ and hPolι show an interesting increase in mutation at roughly 4-5 nucleotides after the lesion. The effect is cyclic for hPolι, with an increase in error frequency every 4-5 nucleotides through the entire sequencing window. Similar downstream effects have been observed for other lesions[40], and we hypothesize that this may be due to an increase DNA structural distortion at each turn of the double helix away from the lesion.

In summary, our study provided further evidence that hPolη is the DNA polymerase that bypasses *cis-syn* cyclobutane thymine dimers *in vivo* due to its high efficiency of lesion bypass. We hope further confirmation will be provided by the sequences of TT dimer lesion bypass products. We observed that hRev1 is not catalytically relevant for TT dimer bypass, though other studies have suggested its role in facilitating polymerase switching for lesion bypass. Our study also supports the hypothesis that hPolι is the DNA polymerase that substitutes for hPolη in humans with XPV because it has decreased lesion bypass efficiency and creates the same mutations observed in XPV cell lines. Finally, we observed the bias of hPolκ for extension of mismatched primer termini by comparing our results to kinetic studies of fidelity, which has application to the proposed role of hPolκ in extending from initial lesion bypass products.

Overall, however, I must reiterate that the data presented herein is preliminary and that further sequences must be collected to verify the statistical validity of our results.

Chapter 3: The Mutagenic Spectra of Cisplatin-dGpG Bypass by Y-family DNA Polymerases

Background

Most damage to cellular DNA is unintentional; a product of the environment that the cell is exposed to. In the case of select chemotherapeutic agents, however, DNA damage is quite intentional. *Cis*-diamminedichloroplatinum(II), also known as cisplatin, is a perfect example. Cisplatin is a chemotherapeutic agent used to treat testicular, ovarian, head, neck, and non-small cell lung cancers. It is an effective anti-cancer agent because it hinders a cell's ability to divide, consequently slowing tumor growth. Cisplatin hinders cell division by creating lesions in DNA that obstruct DNA replication[42]. The most common lesion created by cisplatin treatment is the intrastrand crosslinking of adjacent guanines; often termed a 'cisplatin-dGpG' adduct[42].

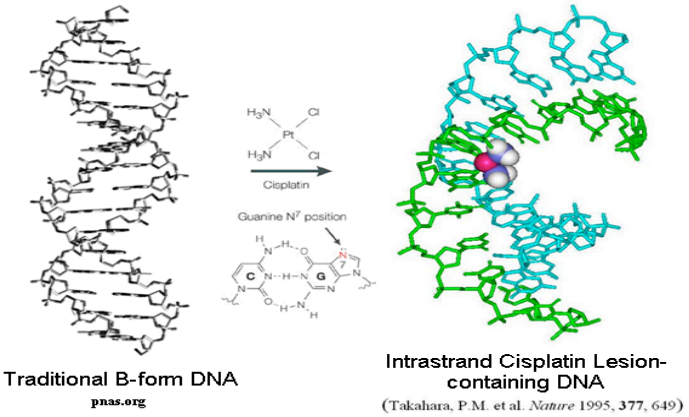

Figure 1. Comparative crystal structures of undamaged DNA and DNA containing a cisplatin-dGpG adduct.

Unfortunately, a major limitation of cisplatin therapy is the prevalence of drug resistance. *In vivo* studies of this dilemma led to the hypothesis that lesion bypass is the mechanism of drug resistance[43], and it is a logical assumption to propose that stalled DNA replication would be responded to in the same way whether the lesion is intentionally or unintentionally introduced. It is therefore important to study cisplatin-dGpG lesion bypass in order to test this hypothesis.

Among the primary candidates to perform cisplatin-dGpG lesion bypass are the Y-family DNA polymerases[42]. Previous studies have focused on hPolη[43-46]. *In vitro* kinetic studies indicate that hPolη preferentially bypasses cisplatin-dGpG lesions in an error-free manner, inserting dCTP opposite both guanines of the adduct. hPolη-deficient (XPV) cell lines also show increased sensitivity to cisplatin; a sensitivity that decreases when the cells are complemented with wild-type hPolη[43]. Though these studies strongly support hPolη's role in cisplatin-dGpG bypass, the ability of other Y-family DNA polymerases to bypass cisplatin-dGpG adducts is largely unknown. Therefore, our goals were 1) to confirm cisplatin-dGpG bypass ability by hPolη, 2) to test the cisplatin-dGpG bypass ability of hPolκ, hPolι, and hRev1, and 3) to characterize the mutagenic profile of lesion bypass by the human Y-family DNA polymerases and the model Y-family member from *Sulfolobus solfataricus*, DNA Polymerase IV (Dpo4).

Methods

Materials: In addition to the reagents mentioned in Chapters 1 and 2, the following were purchased: synthetic deoxyribonucleotide overhang 15-mer with 5'-monophosphate (15-mer P), primer 15-mer, reverse primer 15-mer, 24-mer, 18-mer, 29-mer, 47-mer, and 54-mer control from Integrated DNA Technologies. A 12-mer containing a site-specific cisplatin-dGpG adduct was synthesized previously.

Ligation of 54-mer containing a site-specific cisplatin-dGpG adduct for running start assays: All deoxyribonucleotides received from Integrated DNA Technologies were purified using polyacrylamide gel electrophoresis as in previous chapters. An 18-mer and a 12-mer containing a site-specific cisplatin-dGpG adduct (12-mer CISP) were 5'-phosphorylated as described in Chapter 2. The phosphorylated 18-mer and 12-mer CISP were mixed with 47-mer and 24-mer in a 1.0:1.0:1.0:1.0 molar ratio. Annealing, ligation, and purification of 54-mer CISP were performed in the same manner as the ligation of the 77-mer TT in Chapter 2.

Running Start Assays: For running start assays, primer 15-mer was annealed to 54-mers control and CISP by heating to 95˚C and cooling slowly to room temperature. Running start assays were performed under the same conditions as in Chapter 2.

Ligation of 69-mers control and CISP for short oligonucleotide sequencing assays: In order to separate template DNA from product DNA on a sequencing gel, 69-mers control and CISP were synthesized by adding an overhanging 15-mer to the 54-mers control and CISP. 15-mer P, 54-mer control or CISP, and scaffold 29-mer were mixed at a 1.0:1.0:1.0 molar ratio, heated to 95˚C, and cooled slowly to promote annealing. T4 DNA ligase (NEB) was added according to the manufacturer's directions, and ligation proceeded for 3 hours at 22˚C. The 69-mers control and CISP were purified as described in Chapter 2. Ligation and DNA purification duties were shared between myself and other members of the lab.

Short Oligonucleotide Sequencing Assays:

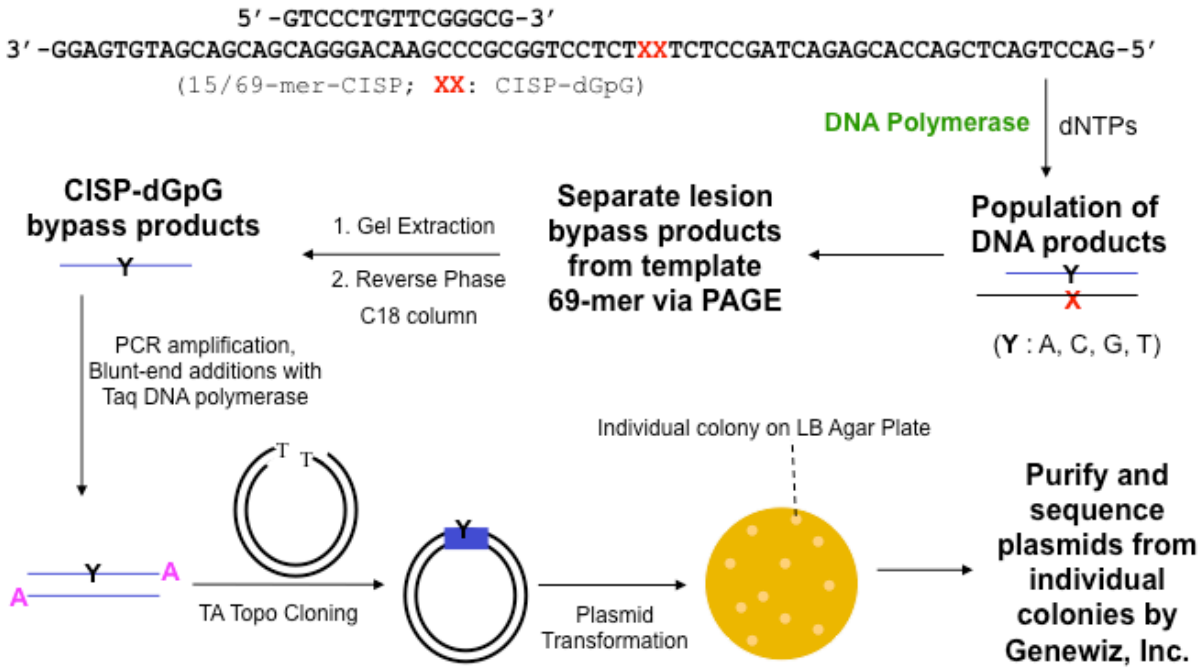

Figure 2. Scheme for short oligonucleotide sequencing assay for cisplatin-dGpG bypass.

For SOSAs, primer 15-mer was annealed to 69-mers control and CISP in the same manner as the 15/54-mers. SOSAs were performed by mixing pre-incubated 15/69-mer control or CISP (120 nM) and Y-family DNA polymerase (30 nM) in buffer "R" with a solution containing all four dNTPs (200 μM). SOSAs were performed for all four human Y-family DNA polymerases and Dpo4; all on both 69-mer control and 69-mer TT. Each reaction proceeded for a time period optimized to maximize the amount of full-length (54-mer) product while minimizing any DNA degradation. To terminate the reaction, the mixture was subjected to 3 freeze-thaw cycles (-196˚C to 95˚C). Full-length 54-mer product was separated from template 69-mer and incompletely replicated deoxyribonucleotides using 10% acrylamide 8M urea gel electrophoresis. The isolated products were amplified using polymerase achain reaction (PCR), aided by *Taq* DNA polymerase, 15-mer forward PCR primer, and 15-mer reverse PCR primer.

These primers were designed to create a sequencing 'window' of 24 bases, including 8 bases prior to the cisplatin-dGpG and 14 bases after cisplatin-dGpG encounter. The population of amplified DNA products were ligated into a pCR4-TOPO vector using a TOPO TA cloning kit (Invitrogen) and transformed into TOP10 *E.coli* (Invitrogen) according to the manufacturer's directions. Individual colonies (each potentially indicative of a different full-length product) were picked and their plasmids sequenced (Genewiz, Inc). I personally performed two SOSAs and optimization assays for several others; the other complete SOSAs were performed previously.

Results

Running start assays: While performing running start assays of human Y-family DNA polymerase and Dpo4 bypass of cisplatin-dGpG adducts, we had two primary goals. First, we intended to confirm that cisplatin-dGpG bypass is possible for hPolη and Dpo4. Second, we aimed to test the ability of hPolι, hPolκ, and hRev1 to bypass cisplatin-dGpG adducts, which was largely unstudied. It was especially beneficial to confirm the ability of hPolη and Dpo4 to perform cisplatin-dGpG bypass under our reaction conditions such that we have a basis for comparison for the untested DNA polymerases.

We observed that all DNA polymerases studied were able to bypass a cisplatin-dGpG adduct to various degrees, as indicated by product past the site of the lesion on the 15/69-mer primer/template DNA containing a site-specific cisplatin-dGpG lesion. For each running start assay performed on 15/69mer-CISP DNA substrate, a similar running assay was performed on 15/69-mer control DNA substrate for comparison.

DNA substrates for running start assays and SOSAs
15/69-mer control
5′-GTCCCTGTTCGGGCG-3′ 3′-GGAGTGTAGCAGCAGCAGGGACAAGCCCGCGGTCCTCTGGTCTCCGATCAGAGCACCAGCTCAGTCCAG-5′
15/69-mer CISP
5′-GTCCCTGTTCGGGCG-3′ 3′-GGAGTGTAGCAGCAGCAGGGACAAGCCCGCGGTCCTCTGGTCTCCGATCAGAGCACCAGCTCAGTCCAG-5′

Table 1. Annealed 15/69-mers for running start assays and SOSAs. The position of the lesion is highlighted in red.

In general, we looked for pause sites on both control and damaged DNA substrates, indicative of polymerase stalling. The following is a brief relation of our observations from the running start assays:

i. hPolη: On control DNA, no significant pausing was observed. On DNA containing a cisplatin-dGpG adduct, heavy pausing was noticed at positions 25 and 26, indicating polymerase stalling upon extension from the cisplatin-dGpG adduct and the subsequent nucleotide incorporation (Appendix 3, Figure 1). We observed lesion bypass products (25-mer) after 2 seconds, and a significant amount of full length product on damaged after 10 seconds. In comparison, we observed 25-mer after 1 second and full length product after 5 seconds on control DNA.

ii. hPolκ: On control and damaged DNA, pausing was observed at positions 16, 20, and 21. All were areas of sequence redundancy (doublet dG, doublet dCdT), which was previously noted to cause polymerase stalling in Chapter 2. hPolκ paused strongly at position 23 on the 69-mer CISP, indicative of polymerase stalling upon incorporation opposite the first dG of the cisplatin adduct. We observed full-length products on damaged DNA after 90 seconds and on

control DNA after 60 seconds. A band indicating lesion bypass product was not obvious on damaged DNA, though full-length product at 90 seconds indicates that the lesion must have been bypassed previously (Appendix 3, Figure 2).

iii. hPolι: Running start assays have not yet been performed for hPolι due to material constraints.

iv. hRev1: Running start assays have not yet been performed for hRev1 due to material constraints.

v. Dpo4: On control DNA, no significant pausing was observed. On DNA containing the cisplatin adduct, pausing was noticed at positions 23 and 24. Pausing at position 24 was far stronger, indicative of polymerase stalling upon incorporation opposite the second dG of the cisplatin adduct. We observed lesion bypass products (25-mer) after 4 seconds and full-length product after 60 seconds on damaged DNA. In comparison, we observed 25-mer after 2 seconds and full-length product after 30 seconds on control DNA (Appendix 3, Figure 3).

Short oligonucleotide sequencing assays: Our goals in performing SOSAs were to profile the mutagenic spectra of cisplatin-dGpG lesion bypass by the human Y-family DNA polymerases and Dpo4. This is instructive because many studies of lesion bypass are only concerned with error frequency *at* the lesion, and do not study mutagenic events upstream and downstream of the lesion. As we have noticed in previous studies, the presence of a lesion can effect upstream and downstream nucleotide incorporation[40]. The following is a summary of our current results from SOSAs:

i. hPolη: Sequence collection is still in progress for hPolη.

ii. hPolκ: On control DNA, hPolκ exhibited a random spectra of mutations except for a notable increase in deletions at position 22, which corresponds to the second dC of a doublet dC. The presence of a cisplatin-dGpG adduct had a dramatic effect on the error frequency of hPolκ, with a sharp increase in deletions for a 9-nucleotide region around the lesion (Appendix 3, Figures 4 and 5).

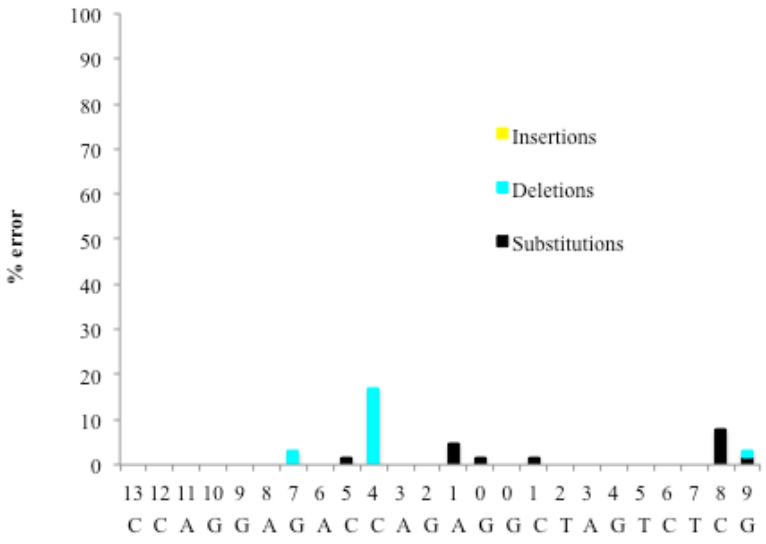

A.

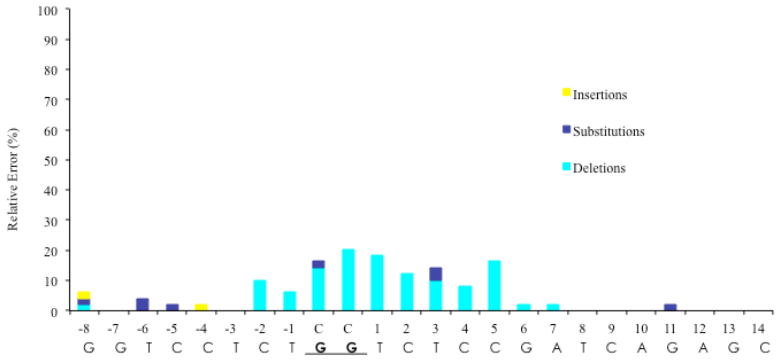

B.

Figure 3. Mutagenic spectra of polymerization by hPolκ on A. 69-mer control DNA and B. 69-mer CISP DNA. The relevant template sequences are denoted below the charts.

iii. hPolι: Sequences have not yet been collected for hPolι.

iv. hRev1: Sequences have not yet been collected for hRev1.

v. Dpo4: On control DNA, Dpo4 exhibited a random spectrum of mutations. Dpo4 exhibited a similar response to a cisplatin-dGpG adduct as hPolκ, displaying an increase in deletion mutations for 7 bases beginning at the site of the lesion (Appendix 3, Figures 6 and 7).

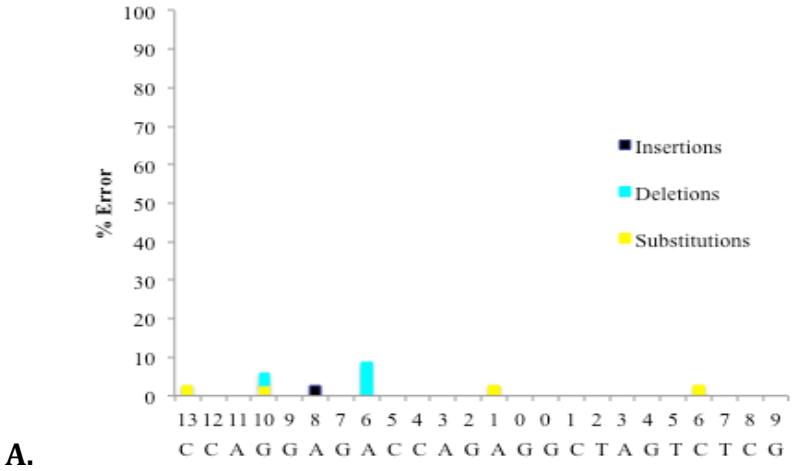

A.

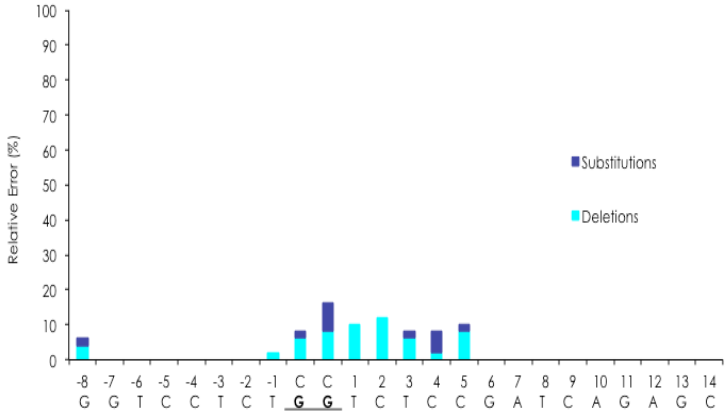

B.

Figure 4. Mutagenic spectra of polymerization by Dpo4 on A. 69-mer control DNA and B. 69-mer CISP DNA. The relevant template sequences are denoted below the charts.

As in Chapter 2, after sequence collection we calculated the total error frequency of polymerization. Both hPolκ and Dpo4 exhibited a 3-fold increase on damaged DNA. Discounting errors at the site of the lesion, total error frequency still increased 3-fold and 2-fold for hPolκ and Dpo4, respectively.

Enzyme	Total Error Frequency (69-mer control)	Total Error Frequency (69-mer CISP)	Total Error Frequency except cisplatin-dGpG site (69-mer CISP)
hPolκ	1.8×10^{-2}	5.8×10^{-2}	4.8×10^{-2}
hPolη	--	--	--
hPolι	--	--	--
hRev1	--	--	--
Dpo4	1.1×10^{-2}	3.1×10^{-2}	2.5×10^{-2}

Table 2. Comparative error frequencies on 15/69-mer control and 15/69-mer CISP.

In summary, we observed that hPolκ, hPolη, and Dpo4 are able to bypass a cisplatin-dGpG adduct. Dpo4 and hPolκ exhibited a similar spectrum of mutations, primarily deletions around the site of the cisplatin-dGpG adduct. hPolη was the most efficient at cisplatin-dGpG bypass. Notably, hPolη generated lesion bypass products after 2 seconds, whereas hPolκ required ~90 seconds and Dpo4 required 4 seconds. Further results are forthcoming.

Discussion

Lesion bypass is an essential process that enables the cell to continue DNA replication past DNA lesions. In tumors treated with cisplatin, a chemotherapeutic agent that harms cancer cells by creating DNA lesions, lesion bypass is a potential mechanism of drug resistance. The Y-

family DNA polymerases are specialized for lesion bypass and are therefore suspected to bypass cisplatin-DNA adducts *in vivo*[41]. In this study, we confirmed the ability of two human Y-family DNA polymerases and a model Y-family DNA polymerase to perform bypass of the most common cisplatin-DNA adduct. We also profiled the mutagenic spectra of cisplatin bypass by a human Y-family DNA polymerase and a model Y-family DNA polymerase. As in Chapter 2, the DNA polymerases studied displayed distinct lesion bypass mechanisms. Below, I will discuss our current results in light of current knowledge of each enzyme.

i. hPolη: We observed that hPolη was able to bypass a cisplatin-dGpG adduct with the highest efficiency of any of the DNA polymerases studied, generating lesion bypass product after 2 seconds. hPolη exhibited the strongest pausing upon extension from the lesion. Previous studies indicate that this pausing may be due to misincorporation opposite the lesion. Kinetic studies noted that when hPolη inserted an incorrect nucleotide opposite the first dG of a cisplatin adduct it was not able to extend[46]. Crystal structures of hPolη in complex with cisplatin-containing DNA and incoming nucleotide suggest a higher propensity for misincorporation opposite G2 rather than G1. It is possible that hPolη is similarly not able to extend from misincorporations opposite G2. The combination of error-prone incorporation opposite G2 and lack of ability to extend from misincorporations may explain the strong pausing seen upon extension from the cisplatin-dGpG adduct[44].

ii. hPolκ: We observed that hPolκ was able to bypass a cisplatin-dGpG adduct, though with a lower efficiency than either hPolη or Dpo4. It had particular difficulty incorporating a nucleotide opposite the first dG of the adduct. This may be due to similar difficulties that hPolκ exhibited on DNA containing a TT dimer in Chapter 2. Notably, hPolκ has the most constrained

active site of any of the human Y-family DNA polymerases[34]. This likely enforces a strict steric requirement that hinders accommodation of the bulky cisplatin lesion. As in TT dimer bypass, hPolκ ably extended from the lesion. This is in accord with its ability to preferentially extend from nucleotides opposite a lesion[35].

The primary change in the mutagenic spectrum of hPolκ due to the presence of a cisplatin-dGpG lesion was an increase in deletion mutations for 9 nucleotides around the site of the lesion. Though never observed for this large a stretch of DNA, previous studies *have* indicated that hPolκ can use primer/template misalignment to extend mismatched primer termini. Primer/template misalignment was the preferred route of mismatch extension when the template base was not present, as in extension from AP sites[47]. It is possible that hPolκ is looping the intervening section containing the cisplatin-dGpG adduct out of its active site, then extending from a severely misaligned template. However, further structural and functional studies are needed to confirm this hypothesis.

iii. Dpo4: We observed that Dpo4, the model Y-family DNA polymerase from *Sulfolobus solfataricus*, was able to efficiently bypass a cisplatin-dGpG lesion, generating bypass product after 4 seconds. Based on our running start assay, it appeared that Dpo4 stalled upon incorporation opposite both dGs of the cisplatin adduct, though more strongly opposite the second dG. Previous pre-steady state kinetic studies confirm this pattern, noting 72-fold and 860-fold decreases in nucleotide incorporation efficiency at the first dG and the second dG, respectively[41]. The ternary crystal structure of Dpo4 in complex with DNA containing a cisplatin-dGpG adduct and incoming nucleotide suggests structural reasons for loss of incorporation efficiency at each position. The first incorporation is hindered by the inability of

the template dG to optimally position itself; instead, it is being dragged towards the major groove by the second dG of the adduct. The second incorporation is hindered by unstable template dG positioning; though the template was observed to position itself optimally, another conformation existed in which template dG was tilted 10˚. This instability was hypothesized to have a greater effect than the non-ideal positioning of the first dG and to account for the dramatic decrease in incorporation efficiency opposite the second dG[48].

The major change in error frequency due to the lesion was an increase in deletion frequency at the cisplatin-dGpG adduct and for the following 5 nucleotides. Interestingly, the aforementioned pre-steady state kinetic studies of Dpo4 bypassing a cisplatin lesion noted a decrease in incorporation efficiency both at the lesion and for six bases downstream[41]. As with hPolκ, we hypothesize that this is due to the structural distortion of DNA due to the presence of a cisplatin lesion. Dpo4, also like hPolκ, has been shown to stabilize primer/template misalignments to generate deletion mutations[49]. Though this was only observed for single base deletions, it is possible that a similar mechanism is being used to delete larger sections as seen in our sequence data.

In summary, we used running start assays and short oligonucleotide sequencing assays to confirm that hPolκ, hPolη, and Dpo4 were able to bypass a cisplatin-dGpG adduct and to sequence the bypass products of hPolκ and Dpo4. hPolη was the most efficient at bypassing the lesion, though it stalled upon extension from the lesion. hPolκ had difficulty incorporating nucleotides opposite the first dG of the lesion, though it ably extended once the first nucleotide was incorporated. Dpo4 paused upon incorporation opposite both nucleotides of the lesion, though more strongly at the second nucleotide due to unstable template positioning. hPolκ and

Dpo4 exhibited similar changes in error frequency in response to the lesion, displaying dramatic increases in deletion mutations at the site of the lesion.

On a final note, I remind the reader that the results related herein are preliminary and that both running start assays and SOSAs remain to be completed on the other human Y-family DNA polymerases.

Conclusion

In Chapter 1, we used pre-steady state kinetic methods to examine the ability of X-family human DNA polymerases lambda (hPolλ) and beta (hPolβ) to fill gaps in DNA. We found that hPolβ is able to maintain its nucleotide selection fidelity as gap size increased, though it suffered a loss of nucleotide incoporation efficiency. hPolλ exhibited the opposite trend, maintaining its nucleotide incorporation efficiency as gap size increased while suffering a loss of nucleotide selection fidelity. We hypothesize that the constant incorporation efficiency of hPolλ is due to its ability to loop downstream template DNA out of its active site while still maintaining contacts with both the primer terminus and the downstream end of the DNA gap. Finally, we determined that the N-terminal domains that differentiate hPolλ from hPolβ serve to downregulate the nucleotide selection fidelity of hPolλ on 2-10 nucleotide gaps.

In Chapter 2, we determined that all of the human Y-family DNA polymerases and Dpo4 were able to bypass a *cis-syn* cyclobutane thymine dimer. hPolη bypassed the lesion most efficiently, in accordance with its proposed *in vivo* role in TT dimer bypass, followed by Dpo4, hPolκ, hPolι, and hRev1. We then sequenced the TT dimer bypass products using SOSAs, which are still in progress. hPolι and Dpo4 frequently skipped the site of the lesion, while hPolκ extended from substitution mutations opposite the lesion. Interestingly, hPolι displayed some of the same characteristic mutations seen in XPV cell lines, indicating it may take the place of hPolη when hPolη is nonfunctional.

In Chapter 3, we also determined that hPolη, hPolκ, and Dpo4 were able to bypass a cisplatin-dGpG adduct. hPolη did so most efficiently, in accord with its proposed role in

cisplatin bypass *in vivo*. hPolκ and Dpo4 tended to skip the site of the lesion, though running start assays once again showed the proficiency of hPolκ at extension from DNA lesions. This study is still in progress, as both running start assays and SOSAs need to be completed to obtain a full summary of cisplatin-dGpG bypass by the human Y-family DNA polymerases.

In short, this thesis details the main projects I worked on as an undergraduate in the Suo laboratory. These projects were mainly under the guidance of Jessica Brown and Shanen Sherrer. In addition to helping me mature as a scientist, I believe that these projects will contribute to our understanding of DNA repair and lesion bypass.

Appendix 1

21-19/	5′-CGCAGCCGTCCAACCAACTCA$_p$CGTCGATCCAATGCCGTCC-3′
41-mer	3′-GCGTCGGCAGGTTGGTTGAGT**C**GCAGCTAGGTTACGGCAGG-5′
21-19/	5′-CGCAGCCGTCCAACCAACTCA $_p$CGTCGATCCAATGCCGTCC-3′
42-mer	3′-GCGTCGGCAGGTTGGTTGAGT**CG**GCAGCTAGGTTACGGCAGG-5′
21-19/	5′-CGCAGCCGTCCAACCAACTCA $_p$CGTCGATCCAATGCCGTCC-3′
43-mer	3′-GCGTCGGCAGGTTGGTTGAGT**CGA**GCAGCTAGGTTACGGCAGG-5′
21-19/	5′-CGCAGCCGTCCAACCAACTCA $_p$CGTCGATCCAATGCCGTCC-3′
44-mer	3′-GCGTCGGCAGGTTGGTTGAGT**CGAG**GCAGCTAGGTTACGGCAGG-5′
21-19/	5′-CGCAGCCGTCCAACCAACTCA $_p$CGTCGATCCAATGCCGTCC-3′
45-mer	3′-GCGTCGGCAGGTTGGTTGAGT**CGAGT**GCAGCTAGGTTACGGCAGG-5′
21-19/	5′-CGCAGCCGTCCAACCAACTCA $_p$CGTCGATCCAATGCCGTCC-3′
46-mer	3′-GCGTCGGCAGGTTGGTTGAGT**CGAGTG**GCAGCTAGGTTACGGCAGG-5′
21-19/	5′-CGCAGCCGTCCAACCAACTCA $_p$CGTCGATCCAATGCCGTCC-3′
47-mer	3′-GCGTCGGCAGGTTGGTTGAGT**CGAGTGC**GCAGCTAGGTTACGGCAGG-5′
21-19/	5′-CGCAGCCGTCCAACCAACTCA $_p$CGTCGATCCAATGCCGTCC-3′
48-mer	3′-GCGTCGGCAGGTTGGTTGAGT**CGAGTGCG**GCAGCTAGGTTACGGCAGG-5′
21-19/	5′-CGCAGCCGTCCAACCAACTCA $_p$CGTCGATCCAATGCCGTCC-3′
49-mer	3′-GCGTCGGCAGGTTGGTTGAGT**CGAGTGCGA**GCAGCTAGGTTACGGCAGG-5′
21-19/	5′-CGCAGCCGTCCAACCAACTCA $_p$CGTCGATCCAATGCCGTCC-3′
50-mer	3′-GCGTCGGCAGGTTGGTTGAGT**CGAGTGCGAC**GCAGCTAGGTTACGGCAGG-5′
21-19T/	5′-CGCAGCCGTCCAACCAACTCA $_p$TGTCGATCCAATGCCGTCC-3′
42-merCGA	3′-GCGTCGGCAGGTTGGTTGAGT**CG**ACAGCTAGGTTACGGCAGG-5′
21-19/	5′-CGCAGCCGTCCAACCAACTCA $_p$CGTCGATCCAATGCCGTCC-3′
42-merCAG	3′-GCGTCGGCAGGTTGGTTGAGT**CA**GCAGCTAGGTTACGGCAGG-5′
21-19/	5′-CGCAGCCGTCCAACCAACTCA $_p$CGTCGATCCAATGCCGTCC-3′
47-merCAT	3′-GCGTCGGCAGGTTGGTTGAGT**CATGTGC**GCAGCTAGGTTACGGCAGG-5′

Table 1. DNA substrates. pDenotes the 5′-end is phosphorylated. Oligonucleotides located in the gap are in bold, and those that were inserted to expand the gap size are underlined.

dNTP	k_p (s^{-1})	K_d (μM)	k_p/K_d ($\mu M^{-1}s^{-1}$)	Efficiency ratio[a]	Fidelity[b]
21-19/41-mer (1-nucleotide gap)					
dGTP	2.7 ± 0.1	1.9 ± 0.2	1.4	-	
dCTP	0.00145 ± 0.00005	1.0 ± 0.1	1.5×10^{-3}	-	1.0×10^{-3}
dATP	0.00047 ± 0.00002	0.9 ± 0.1	5.2×10^{-4}	-	3.7×10^{-4}
dTTP	0.00135 ± 0.00009	2.9 ± 0.6	4.7×10^{-4}	-	3.3×10^{-4}
21-19/42-mer (2-nucleotide gap)					
dGTP	1.77 ± 0.02	1.51 ± 0.06	1.2	1	
dCTP	0.0161 ± 0.0004	0.69 ± 0.08	2.3×10^{-2}	16 ↑	2.0×10^{-2}
dATP	0.00037 ± 0.00002	1.2 ± 0.2	3.1×10^{-4}	2 ↑	2.6×10^{-4}
dTTP	0.00070 ± 0.00003	3.8 ± 0.5	1.8×10^{-4}	3 ↑	1.6×10^{-4}
21-19/43-mer (3-nucleotide gap)					
dGTP	1.99 ± 0.06	1.5 ± 0.2	1.3	1	
dCTP	0.0079 ± 0.0002	0.79 ± 0.08	1.0×10^{-2}	7 ↑	7.5×10^{-3}
dATP	0.00044 ± 0.00003	0.6 ± 0.2	7.3×10^{-4}	1	5.5×10^{-4}
dTTP	0.00095 ± 0.00008	2.8 ± 0.8	3.4×10^{-4}	1	2.6×10^{-4}
21-19/44-mer (4-nucleotide gap)					
dGTP	1.64 ± 0.03	1.6 ± 0.1	1.0	1	
dCTP	0.0247 ± 0.0006	0.8 ± 0.1	3.1×10^{-2}	21 ↑	2.9×10^{-2}
dATP	0.00126 ± 0.00004	0.48 ± 0.07	2.6×10^{-3}	5 ↑	2.6×10^{-3}
dTTP	0.00129 ± 0.00007	2.8 ± 0.5	4.6×10^{-4}	1	4.5×10^{-4}
21-19/45-mer (5-nucleotide gap)					
dGTP	2.15 ± 0.06	1.6 ± 0.2	1.3	1	
dCTP	0.053 ± 0.001	0.9 ± 0.1	5.9×10^{-2}	41 ↑	4.2×10^{-2}
dATP	0.0031 ± 0.0001	0.54 ± 0.07	5.7×10^{-3}	11 ↑	4.3×10^{-3}
dTTP	0.0118 ± 0.0006	2.7 ± 0.4	4.4×10^{-3}	9 ↑	3.2×10^{-3}
21-19/46-mer (6-nucleotide gap)					
dGTP	1.53 ± 0.06	0.7 ± 0.1	2.2	2 ↑	
dCTP	0.0450 ± 0.0008	0.79 ± 0.07	5.7×10^{-2}	39 ↑	2.5×10^{-2}
dATP	0.00149 ± 0.00002	0.46 ± 0.03	3.2×10^{-3}	6 ↑	1.5×10^{-3}
dTTP	0.0115 ± 0.0003	2.0 ± 0.2	5.8×10^{-3}	12 ↑	2.6×10^{-3}
21-19/47-mer (7-nucleotide gap)					
dGTP	1.86 ± 0.04	1.2 ± 0.1	1.6	1	
dCTP	0.049 ± 0.001	0.9 ± 0.1	5.4×10^{-2}	38 ↑	3.4×10^{-2}
dATP	0.00066 ± 0.00001	0.24 ± 0.02	2.8×10^{-3}	5 ↑	1.8×10^{-3}
dTTP	0.0051 ± 0.0002	1.1 ± 0.2	4.6×10^{-3}	10 ↑	3.0×10^{-3}
21-19/48-mer (8-nucleotide gap)					
dGTP	1.01 ± 0.03	1.6 ± 0.2	0.6	2 ↓	
dCTP	0.0082 ± 0.0002	0.47 ± 0.06	1.7×10^{-2}	12 ↑	2.7×10^{-2}
dATP	0.00023 ± 0.00001	0.8 ± 0.2	2.9×10^{-4}	2 ↓	4.6×10^{-4}
dTTP	0.00072 ± 0.00002	5.1 ± 0.4	1.4×10^{-4}	3 ↓	2.2×10^{-4}
21-19/49-mer (9-nucleotide gap)					
dGTP	0.83 ± 0.03	3.0 ± 0.3	0.3	5 ↓	
dCTP	0.00226 ± 0.00005	0.38 ± 0.05	5.9×10^{-3}	4 ↓	2.1×10^{-2}

dATP	No incorporation				
dTTP	No incorporation				
21-19/50-mer (10-nucleotide gap)					
dGTP	0.026 ± 0.001	0.7 ± 0.1	3.7×10^{-2}	38 ↓	
dCTP	0.00164 ± 0.00007	1.1 ± 0.2	1.5×10^{-3}	1	3.9×10^{-2}
dATP	No incorporation				
dTTP	No incorporation				
21/41-mer (no gap)					
dGTP	0.0353 ± 0.0008	0.82 ± 0.08	4.3×10^{-2}	33 ↓	
dCTP	0.00044 ± 0.00003	3.0 ± 0.7	1.5×10^{-4}	10 ↓	3.4×10^{-3}
dATP	No incorporation				
dTTP	No incorporation				

Table 2. Kinetic parameters for nucleotide incorporation into gapped and recessed DNA catalyzed by hPolλ at 37˚C.

[a]An upward-pointing arrow (↑) indicates the ratio was calculated as $(k_p/K_d)_{\geq 2\text{-nucleotide gap}}/(k_p/K_d)_{1\text{-nucleotide gap}}$; a downward-pointing arrow (↓) indicates the calculation used a reciprocal of the equation as follows: $(k_p/K_d)_{1\text{-nucleotide gap}}/(k_p/K_d)_{\geq 2\text{-nucleotide gap}}$.

[b]Calculated as $(k_p/K_d)_{\text{incorrect}}/[(k_p/K_d)_{\text{correct}} + (k_p/K_d)_{\text{incorrect}}]$.

dNTP	k_p (s^{-1})	K_d (μM)	k_p/K_d ($\mu M^{-1}s^{-1}$)	Efficiency ratio[a]	Fidelity[b]
21-19/41mer (1-nucleotide gap)					
dGTP	3.1 ± 0.1	1.7 ± 0.2	1.8	-	
dCTP	0.00135 ± 0.00007	1.9 ± 0.4	7.1×10^{-4}	-	3.9×10^{-4}
dATP	0.00066 ± 0.00007	1.8 ± 0.7	3.7×10^{-4}	-	2.0×10^{-4}
dTTP	0.00130 ± 0.00009	7 ± 1	1.9×10^{-4}	-	1.0×10^{-4}
21-19/42mer (2-nucleotide gap)					
dGTP	2.80 ± 0.05	1.24 ± 0.09	2.3	1	
dCTP	0.0208 ± 0.0005	0.85 ± 0.09	2.4×10^{-2}	34 ↑	1.1×10^{-2}
dATP	0.00031 ± 0.00002	3.0 ± 0.6	1.0×10^{-4}	4 ↓	4.6×10^{-5}
dTTP	0.00070 ± 0.00004	4.6 ± 0.7	1.5×10^{-4}	1	6.7×10^{-5}
21-19/45mer (5-nucleotide gap)					
dGTP	3.83 ± 0.06	1.57 ± 0.09	2.4	1	
dCTP	0.0060 ± 0.0003	1.5 ± 0.2	4.0×10^{-3}	6 ↑	1.6×10^{-3}
dATP	0.00042 ± 0.00003	3.3 ± 0.6	1.3×10^{-4}	3 ↓	5.2×10^{-5}
dTTP	0.00154 ± 0.00009	7 ± 1	2.2×10^{-4}	1	9.0×10^{-5}
21-19/47mer (7-nucleotide gap)					
dGTP	2.62 ± 0.05	1.28 ± 0.09	2.0	1	
dCTP	0.0072 ± 0.0002	0.77 ± 0.07	9.4×10^{-3}	13 ↑	4.5×10^{-3}
dATP	0.000102 ± 0.000008	2.1 ± 0.5	4.9×10^{-5}	8 ↓	2.4×10^{-5}
dTTP	0.0006 ± 0.0001	6 ± 3	1.0×10^{-4}	2 ↓	4.9×10^{-5}
21-19/50mer (10-nucleotide gap)					
dGTP	0.27 ± 0.01	2.4 ± 0.3	1.1×10^{-1}	16 ↓	
dCTP	0.00019 ± 0.00001	5 ± 1	3.8×10^{-5}	19 ↓	3.4×10^{-4}
dATP	No incorporation				
dTTP	No incorporation				
21/41mer (no gap)					
dGTP	0.109 ± 0.007	1.7 ± 0.3	6.4×10^{-2}	28 ↓	
dCTP	0.00030 ± 0.00002	4.2 ± 0.7	7.1×10^{-5}	10 ↓	1.1×10^{-3}
dATP	No incorporation				
dTTP	No incorporation				

Table 3. Kinetic parameters for nucleotide incorporation into gapped and recessed DNA catalyzed by dPolλ at 37˚C.

[a]An upward-pointing arrow (↑) indicates the ratio was calculated as $(k_p/K_d)_{\geq 2\text{-nucleotide gap}}/(k_p/K_d)_{1\text{-nucleotide gap}}$; a downward-pointing arrow (↓) indicates the calculation used a reciprocal of the equation as follows: $(k_p/K_d)_{1\text{-nucleotide gap}}/(k_p/K_d)_{\geq 2\text{-nucleotide gap}}$.

[b]Calculated as $(k_p/K_d)_{\text{incorrect}}/[(k_p/K_d)_{\text{correct}} + (k_p/K_d)_{\text{incorrect}}]$.

dNTP	k_p (s^{-1})	K_d (μM)	k_p/K_d ($\mu M^{-1}s^{-1}$)	Efficiency ratio[a]	Fidelity[b]
21-19/41mer (1-nucleotide gap)					
dGTP	18.8 ± 0.4	8.7 ± 0.4	2.2	-	
dCTP	0.059 ± 0.002	140 ± 20	4.2×10^{-4}	-	1.9×10^{-4}
dATP	0.32 ± 0.02	280 ± 60	1.1×10^{-3}	-	5.3×10^{-4}
dTTP	0.27 ± 0.01	330 ± 40	8.2×10^{-4}	-	3.7×10^{-4}
21-19/42mer (2-nucleotide gap)					
dGTP	39 ± 1	12 ± 2	3.3	1	
dCTP	0.0153 ± 0.0002	34 ± 3	4.5×10^{-4}	1	1.4×10^{-4}
dATP	0.212 ± 0.009	200 ± 20	1.1×10^{-3}	1	3.3×10^{-4}
dTTP	0.173 ± 0.009	340 ± 50	5.1×10^{-4}	2 ↓	1.6×10^{-4}
21-19/45mer (5-nucleotide gap)					
dGTP	36 ± 2	100 ± 10	3.6×10^{-1}	6 ↓	
dCTP	0.065 ± 0.002	450 ± 30	1.4×10^{-4}	3 ↓	4.0×10^{-4}
dATP	0.0188 ± 0.0006	540 ± 40	3.5×10^{-5}	33 ↓	9.7×10^{-5}
dTTP	0.0117 ± 0.0008	900 ± 100	1.3×10^{-5}	63 ↓	3.6×10^{-5}
21-19/47mer (7-nucleotide gap)					
dGTP	37 ± 5	100 ± 30	3.7×10^{-1}	6 ↓	
dCTP	0.203 ± 0.006	500 ± 40	4.1×10^{-4}	1	1.1×10^{-3}
dATP	0.013 ± 0.002	800 ± 300	1.6×10^{-5}	70 ↓	4.4×10^{-5}
dTTP	0.0096 ± 0.0005	1400 ± 100	6.9×10^{-6}	120 ↓	1.9×10^{-5}
21-19/50mer (10-nucleotide gap)					
dGTP	10.5 ± 0.6	780 ± 90	1.3×10^{-2}	160 ↓	
dCTP	0.0023 ± 0.0001	580 ± 60	4.0×10^{-6}	110 ↓	2.9×10^{-4}
dATP	0.00166 ± 0.00009	440 ± 60	3.8×10^{-6}	300 ↓	2.8×10^{-4}
dTTP	0.00090 ± 0.00006	620 ± 90	1.5×10^{-6}	560 ↓	1.1×10^{-4}
21/41mer (no gap)					
dGTP	31.4 ± 0.6	48 ± 2	6.5×10^{-1}	3 ↓	
dCTP	0.024 ± 0.001	230 ± 30	1.0×10^{-4}	4 ↓	1.6×10^{-4}
dATP	0.111 ± 0.007	650 ± 90	1.7×10^{-4}	7 ↓	2.6×10^{-4}
dTTP	0.094 ± 0.005	1100 ± 100	8.5×10^{-5}	10 ↓	1.3×10^{-4}

Table 4. Kinetic parameters for nucleotide incorporation into gapped and recessed DNA catalyzed by hPolβ at 37˚C.

[a]An upward-pointing arrow (↑) indicates the ratio was calculated as $(k_p/K_d)_{\geq 2\text{-nucleotide gap}}/(k_p/K_d)_{1\text{-nucleotide gap}}$; a downward-pointing arrow (↓) indicates the calculation used a reciprocal of the equation as follows: $(k_p/K_d)_{1\text{-nucleotide gap}}/(k_p/K_d)_{\geq 2\text{-nucleotide gap}}$.

[b]Calculated as $(k_p/K_d)_{\text{incorrect}}/[(k_p/K_d)_{\text{correct}} + (k_p/K_d)_{\text{incorrect}}]$.

dNTP	k_p (s^{-1})	K_d (μM)	k_p/K_d ($\mu M^{-1}s^{-1}$)	Efficiency ratio[a]	Fidelity[b]
21-19/41mer (1-nucleotide gap)[c]					
dGTP	4.1 ± 0.2	1.9 ± 0.4	2.2	-	
dCTP	0.0098 ± 0.0002	1.5 ± 0.2	6.5×10^{-3}	-	3.0×10^{-3}
dATP	0.0046 ± 0.0001	1.4 ± 0.3	3.3×10^{-3}	-	1.5×10^{-3}
dTTP	0.0065 ± 0.0001	4.7 ± 0.5	1.4×10^{-3}	-	6.4×10^{-4}
21-19/42mer (2-nucleotide gap)					
dGTP	3.7 ± 0.2	2.3 ± 0.3	1.6	1	
dCTP	0.081 ± 0.001	1.12 ± 0.07	7.2×10^{-2}	11 ↑	4.3×10^{-2}
dATP	0.0019 ± 0.0002	2.4 ± 0.6	7.9×10^{-4}	4 ↓	4.9×10^{-4}
dTTP	0.0030 ± 0.0009	6 ± 3	5.0×10^{-4}	3 ↓	3.1×10^{-4}
21-19/45mer (5-nucleotide gap)					
dGTP	5.1 ± 0.2	3.3 ± 0.4	1.5	1	
dCTP	0.0123 ± 0.0003	1.4 ± 0.1	8.8×10^{-3}	1	5.7×10^{-3}
dATP	0.0011 ± 0.0002	2 ± 1	5.5×10^{-4}	6 ↓	3.6×10^{-4}
dTTP	0.006 ± 0.002	9 ± 4	6.7×10^{-4}	2 ↓	4.3×10^{-4}
21-19/47mer (7-nucleotide gap)					
dGTP	3.78 ± 0.08	2.5 ± 0.2	1.5	1	
dCTP	0.028 ± 0.002	3.5 ± 0.8	8.0×10^{-3}	1	5.3×10^{-3}
dATP	0.00035 ± 0.00002	1.6 ± 0.4	2.2×10^{-4}	15 ↓	1.4×10^{-4}
dTTP	0.0027 ± 0.0002	11 ± 2	2.5×10^{-4}	6 ↓	1.6×10^{-4}
21-19/50mer (10-nucleotide gap)					
dGTP	1.43 ± 0.05	5.1 ± 0.4	2.8×10^{-1}	8 ↓	
dCTP	0.00067 ± 0.00006	5 ± 1	1.3×10^{-4}	49 ↓	4.8×10^{-4}
dATP	0.000350 ± 0.000009	3.6 ± 0.3	9.7×10^{-5}	34 ↓	3.5×10^{-4}
dTTP	No incorporation				
21/41mer (no gap)					
dGTP	0.68 ± 0.02	2.0 ± 0.2	3.4×10^{-1}	6 ↓	
dCTP	0.0007 ± 0.0001	5 ± 2	1.4×10^{-4}	47 ↓	4.1×10^{-4}
dATP	No incorporation				
dTTP	No incorporation				

Table 5. Kinetic parameters for nucleotide incorporation into gapped and recessed DNA catalyzed by tPolλ at 37˚C.

[a]An upward-pointing arrow (↑) indicates the ratio was calculated as $(k_p/K_d)_{\geq 2\text{-nucleotide gap}}/(k_p/K_d)_{1\text{-nucleotide gap}}$; a downward-pointing arrow (↓) indicates the calculation used a reciprocal of the equation as follows: $(k_p/K_d)_{1\text{-nucleotide gap}}/(k_p/K_d)_{\geq 2\text{-nucleotide gap}}$.

[b]Calculated as $(k_p/K_d)_{\text{incorrect}}/[(k_p/K_d)_{\text{correct}} + (k_p/K_d)_{\text{incorrect}}]$.

dNTP	k_p (s^{-1})	K_d (μM)	k_p/K_d ($\mu M^{-1}s^{-1}$)	Efficiency ratio[a]	Fidelity[b]
21-19/41mer (1-nucleotide gap)					
dGTP	2.7 ± 0.1	1.9 ± 0.2	1.4	-	
dCTP	0.00145 ± 0.00005	1.0 ± 0.1	1.5×10^{-3}	-	1.0×10^{-3}
dATP	0.00047 ± 0.00002	0.9 ± 0.1	5.2×10^{-4}	-	3.7×10^{-4}
dTTP	0.00135 ± 0.00009	2.9 ± 0.6	4.7×10^{-4}	-	3.3×10^{-4}
21-19/42mer (2-nucleotide gap)					
dGTP	1.77 ± 0.02	1.51 ± 0.06	1.2	1	
dCTP	0.0161 ± 0.0004	0.69 ± 0.08	2.3×10^{-2}	16 ↑	2.0×10^{-2}
dATP	0.00037 ± 0.00002	1.2 ± 0.2	3.1×10^{-4}	2 ↓	2.6×10^{-4}
dTTP	0.00070 ± 0.00003	3.8 ± 0.5	1.8×10^{-4}	3 ↓	1.6×10^{-4}
21-19T/42merCGA (2-nucleotide gap)					
dGTP	2.4 ± 0.1	2.4 ± 0.4	1	1	
dCTP	0.0305 ± 0.0007	0.52 ± 0.06	5.9×10^{-2}	40 ↑	5.5×10^{-2}
dATP	0.00069 ± 0.00003	0.6 ± 0.1	1.2×10^{-3}	2 ↑	1.1×10^{-3}
dTTP	0.00075 ± 0.00004	3.3 ± 0.7	2.3×10^{-4}	2 ↓	2.3×10^{-4}
21-19/42merCAG (2-nucleotide gap)					
dGTP	2.9 ± 0.1	1.7 ± 0.3	1.7	1	
dCTP	0.00076 ± 0.00007	1.7 ± 0.5	4.5×10^{-4}	3 ↓	2.6×10^{-4}
dATP	0.00049 ± 0.00002	0.9 ± 0.2	5.4×10^{-4}	1	3.2×10^{-4}
dTTP	0.0025 ± 0.0002	4.4 ± 0.8	5.7×10^{-4}	1	3.3×10^{-4}
21-19/47mer (7-nucleotide gap)					
dGTP	1.86 ± 0.04	1.2 ± 0.1	1.6	1	
dCTP	0.049 ± 0.001	0.9 ± 0.1	5.4×10^{-2}	38 ↑	3.4×10^{-2}
dATP	0.00066 ± 0.00001	0.24 ± 0.02	2.8×10^{-3}	5 ↑	1.8×10^{-3}
dTTP	0.0051 ± 0.0002	1.1 ± 0.2	4.6×10^{-3}	10 ↑	3.0×10^{-3}
21-19/47merCAT (7-nucleotide gap)					
dGTP	3.3 ± 0.2	3.1 ± 0.6	1.1	1	
dCTP	0.0087 ± 0.0001	0.58 ± 0.03	1.5×10^{-2}	10 ↑	1.4×10^{-2}
dATP	0.0045 ± 0.0001	1.2 ± 0.1	3.8×10^{-3}	7 ↑	3.5×10^{-3}
dTTP	0.146 ± 0.002	2.5 ± 0.1	5.8×10^{-2}	125 ↑	5.2×10^{-2}

Table 6. Kinetic parameters for nucleotide incorporation into gapped DNA catalyzed by hPolλ at 37˚C.

[a]An upward-pointing arrow (↑) indicates the ratio was calculated as $(k_p/K_d)_{\geq 2\text{-nucleotide gap}}/(k_p/K_d)_{1\text{-nucleotide gap}}$; a downward-pointing arrow (↓) indicates the calculation used a reciprocal of the equation as follows: $(k_p/K_d)_{1\text{-nucleotide gap}}/(k_p/K_d)_{\geq 2\text{-nucleotide gap}}$.

[b]Calculated as $(k_p/K_d)_{\text{incorrect}}/[(k_p/K_d)_{\text{correct}} + (k_p/K_d)_{\text{incorrect}}]$.

dNTP	k_p (s^{-1})	K_d (μM)	k_p/K_d ($\mu M^{-1}s^{-1}$)	Efficiency ratio[a]	Fidelity[b]
21-19/41mer (1-nucleotide gap)					
dGTP	18.8 ± 0.4	8.7 ± 0.4	2.2	-	
dCTP	0.059 ± 0.002	140 ± 20	4.2×10^{-4}	-	1.9×10^{-4}
dATP	0.32 ± 0.02	280 ± 60	1.1×10^{-3}	-	5.3×10^{-4}
dTTP	0.27 ± 0.01	330 ± 40	8.2×10^{-4}	-	3.7×10^{-4}
21-19/42mer (2-nucleotide gap)					
dGTP	39 ± 1	12 ± 2	3.3	1	
dCTP	0.0153 ± 0.0002	34 ± 3	4.5×10^{-4}	1	1.4×10^{-4}
dATP	0.212 ± 0.009	200 ± 20	1.1×10^{-3}	1	3.3×10^{-4}
dTTP	0.173 ± 0.009	340 ± 50	5.1×10^{-4}	2 ↓	1.6×10^{-4}
21-19T/42merCGA (2-nucleotide gap)					
dGTP	41 ± 4	10 ± 3	4.1	2 ↑	
dCTP	0.041 ± 0.006	300 ± 100	1.4×10^{-4}	3 ↓	3.3×10^{-5}
dATP	0.094 ± 0.005	190 ± 30	4.9×10^{-4}	2 ↓	1.2×10^{-4}
dTTP	0.26 ± 0.07	1500 ± 600	1.7×10^{-4}	5 ↓	4.2×10^{-5}
21-19/42merCAG (2-nucleotide gap)					
dGTP	44 ± 1	10 ± 1	4.4	2 ↑	
dCTP	0.072 ± 0.004	340 ± 60	2.1×10^{-4}	2 ↓	4.8×10^{-5}
dATP	0.180 ± 0.008	140 ± 20	1.3×10^{-3}	1	2.9×10^{-4}
dTTP	0.0103 ± 0.0003	17 ± 2	6.1×10^{-4}	1	1.4×10^{-4}
21-19/47mer (7-nucleotide gap)					
dGTP	37 ± 5	100 ± 30	3.7×10^{-1}	6 ↓	
dCTP	0.203 ± 0.006	500 ± 40	4.1×10^{-4}	1	1.1×10^{-3}
dATP	0.013 ± 0.002	800 ± 300	1.6×10^{-5}	70 ↓	4.4×10^{-5}
dTTP	0.0096 ± 0.0005	1400 ± 100	6.9×10^{-6}	120 ↓	1.9×10^{-5}
21-19/47merCAT (7-nucleotide gap)					
dGTP	32 ± 4	230 ± 60	1.4×10^{-1}	16 ↓	
dCTP	0.0116 ± 0.0009	1200 ± 200	9.7×10^{-6}	44 ↓	6.9×10^{-5}
dATP	0.04 ± 0.01	1300 ± 700	3.1×10^{-5}	37 ↓	2.2×10^{-4}
dTTP	0.0113 ± 0.0003	850 ± 40	1.3×10^{-5}	62 ↓	9.6×10^{-5}

Table 7. Kinetic parameters for nucleotide incorporation into gapped DNA catalyzed by hPolβ at 37˚C.

[a]An upward-pointing arrow (↑) indicates the ratio was calculated as $(k_p/K_d)_{\geq 2\text{-nucleotide gap}}/(k_p/K_d)_{1\text{-nucleotide gap}}$; a downward-pointing arrow (↓) indicates the calculation used a reciprocal of the equation as follows: $(k_p/K_d)_{1\text{-nucleotide gap}}/(k_p/K_d)_{\geq 2\text{-nucleotide gap}}$.

[b]Calculated as $(k_p/K_d)_{\text{incorrect}}/[(k_p/K_d)_{\text{correct}} + (k_p/K_d)_{\text{incorrect}}]$.

dNTP	k_p (s^{-1})	K_d (μM)	k_p/K_d ($\mu M^{-1}s^{-1}$)	Efficiency ratio[a]	Fidelity[b]
21-19/41mer (1-nucleotide gap)					
dGTP	3.1 ± 0.1	1.7 ± 0.2	1.8	-	
dCTP	0.00135 ± 0.00007	1.9 ± 0.4	7.1×10^{-4}	-	3.9×10^{-4}
dATP	0.00066 ± 0.00007	1.8 ± 0.7	3.7×10^{-4}	-	2.0×10^{-4}
dTTP	0.00130 ± 0.00009	7 ± 1	1.9×10^{-4}	-	1.0×10^{-4}
21-19/42mer (2-nucleotide gap)					
dGTP	2.80 ± 0.05	1.24 ± 0.09	2.3	1	
dCTP	0.0208 ± 0.0005	0.85 ± 0.09	2.4×10^{-2}	34 ↑	1.1×10^{-2}
dATP	0.00031 ± 0.00002	3.0 ± 0.6	1.0×10^{-4}	4 ↓	4.6×10^{-5}
dTTP	0.00070 ± 0.00004	4.6 ± 0.7	1.5×10^{-4}	1	6.7×10^{-5}
21-19T/42merCGA (2-nucleotide gap)					
dGTP	2.57 ± 0.08	0.9 ± 0.1	2.9	1	
dCTP	0.0200 ± 0.0006	0.80 ± 0.07	2.5×10^{-2}	35 ↑	8.7×10^{-3}
dATP	0.00027 ± 0.00002	1.3 ± 0.4	2.1×10^{-4}	2 ↓	7.3×10^{-5}
dTTP	0.00024 ± 0.00002	3.3 ± 0.8	7.3×10^{-5}	3 ↓	2.5×10^{-5}
21-19/42merCAG (2-nucleotide gap)					
dGTP	3.9 ± 0.2	1.6 ± 0.3	2.4	1	
dCTP	0.00116 ± 0.00008	2.3 ± 0.5	5.0×10^{-4}	1	2.1×10^{-4}
dATP	0.00030 ± 0.00003	2.5 ± 0.8	1.2×10^{-4}	3 ↓	4.9×10^{-5}
dTTP	0.0027 ± 0.0002	4.0 ± 0.9	6.8×10^{-4}	4 ↑	2.8×10^{-4}

Table 8. Kinetic parameters for nucleotide incorporation into gapped DNA catalyzed by dPolλ at 37˚C.

[a]An upward-pointing arrow (↑) indicates the ratio was calculated as $(k_p/K_d)_{\geq 2\text{-nucleotide gap}}/(k_p/K_d)_{1\text{-nucleotide gap}}$; a downward-pointing arrow (↓) indicates the calculation used a reciprocal of the equation as follows: $(k_p/K_d)_{1\text{-nucleotide gap}}/(k_p/K_d)_{\geq 2\text{-nucleotide gap}}$.

[b]Calculated as $(k_p/K_d)_{\text{incorrect}}/[(k_p/K_d)_{\text{correct}} + (k_p/K_d)_{\text{incorrect}}]$.

dNTP	k_p (s^{-1})	K_d (μM)	k_p/K_d ($\mu M^{-1}s^{-1}$)	Efficiency ratio[a]	Fidelity[b]
21-19/41mer (1-nucleotide gap)[c]					
dGTP	4.1 ± 0.2	1.9 ± 0.4	2.2	-	
dCTP	0.0098 ± 0.0002	1.5 ± 0.2	6.5×10^{-3}	-	3.0×10^{-3}
dATP	0.0046 ± 0.0001	1.4 ± 0.3	3.3×10^{-3}	-	1.5×10^{-3}
dTTP	0.0065 ± 0.0001	4.7 ± 0.5	1.4×10^{-3}	-	6.4×10^{-4}
21-19T/42mer (2-nucleotide gap)					
dGTP	3.7 ± 0.2	2.3 ± 0.3	1.6	1	
dCTP	0.081 ± 0.001	1.12 ± 0.07	7.2×10^{-2}	11 ↑	4.3×10^{-2}
dATP	0.0019 ± 0.0002	2.4 ± 0.6	7.9×10^{-4}	4 ↓	4.9×10^{-4}
dTTP	0.0030 ± 0.0009	6 ± 3	5.0×10^{-4}	3 ↓	3.1×10^{-4}
21-19/42merCGA (2-nucleotide gap)					
dGTP	4.8 ± 0.1	2.1 ± 0.2	2.3	1	
dCTP	0.141 ± 0.003	0.78 ± 0.06	1.8×10^{-1}	28 ↑	7.3×10^{-2}
dATP	0.0014 ± 0.0001	1.3 ± 0.3	1.1×10^{-3}	3 ↓	4.7×10^{-4}
dTTP	0.0028 ± 0.0002	5 ± 2	5.6×10^{-4}	2 ↓	2.4×10^{-4}
21-19/42merCAG (2-nucleotide gap)					
dGTP	4.6 ± 0.2	2.6 ± 0.4	1.8	1	
dCTP	0.0064 ± 0.0003	1.3 ± 0.2	4.9×10^{-3}	1	2.8×10^{-3}
dATP	0.002 ± 0.0001	1.3 ± 0.3	1.5×10^{-3}	2 ↓	8.7×10^{-4}
dTTP	0.016 ± 0.001	4.3 ± 0.9	3.7×10^{-3}	3 ↑	2.1×10^{-3}

Table 9. Kinetic parameters for nucleotide incorporation into gapped DNA catalyzed by tPolλ at 37˚C.

[a]An upward-pointing arrow (↑) indicates the ratio was calculated as $(k_p/K_d)_{\geq 2\text{-nucleotide gap}}/(k_p/K_d)_{1\text{-nucleotide gap}}$; a downward-pointing arrow (↓) indicates the calculation used a reciprocal of the equation as follows: $(k_p/K_d)_{1\text{-nucleotide gap}}/(k_p/K_d)_{\geq 2\text{-nucleotide gap}}$.

[b]Calculated as $(k_p/K_d)_{\text{incorrect}}/[(k_p/K_d)_{\text{correct}} + (k_p/K_d)_{\text{incorrect}}]$.

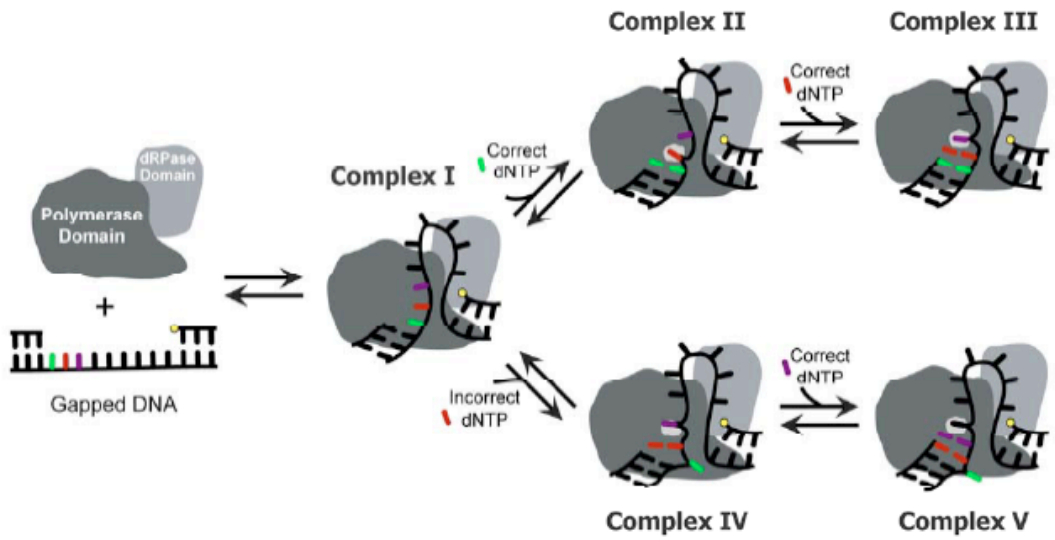

Figure 1. Model of template scrunching and stabilization of misalignment by hPolλ.

Appendix 2

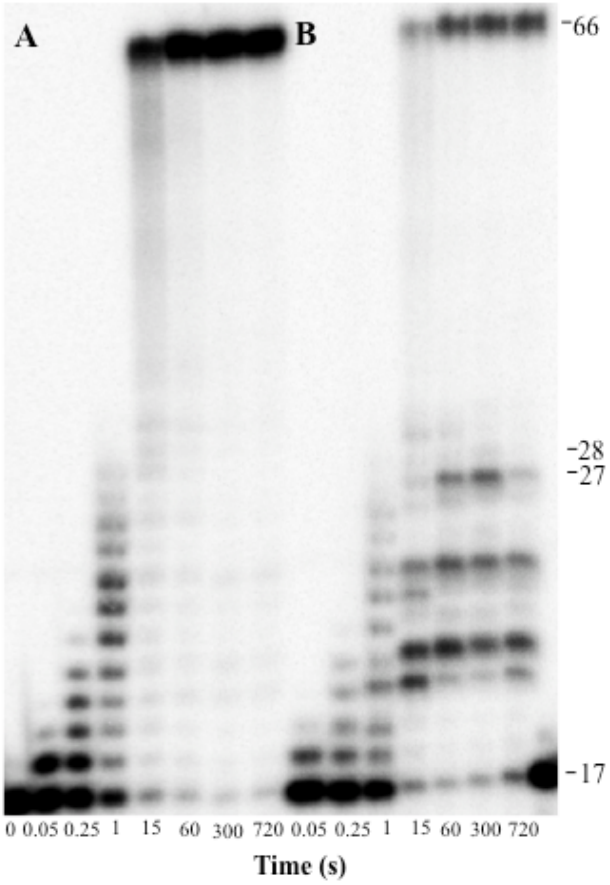

Figure 1. A. Running start assay of hPolη on 17/77-mer control, B. On 17/77-mer TT. "17" denotes the primer band, "27" T1 of the TT dimer, "28" T2 of the TT dimer, and "66" full length product.

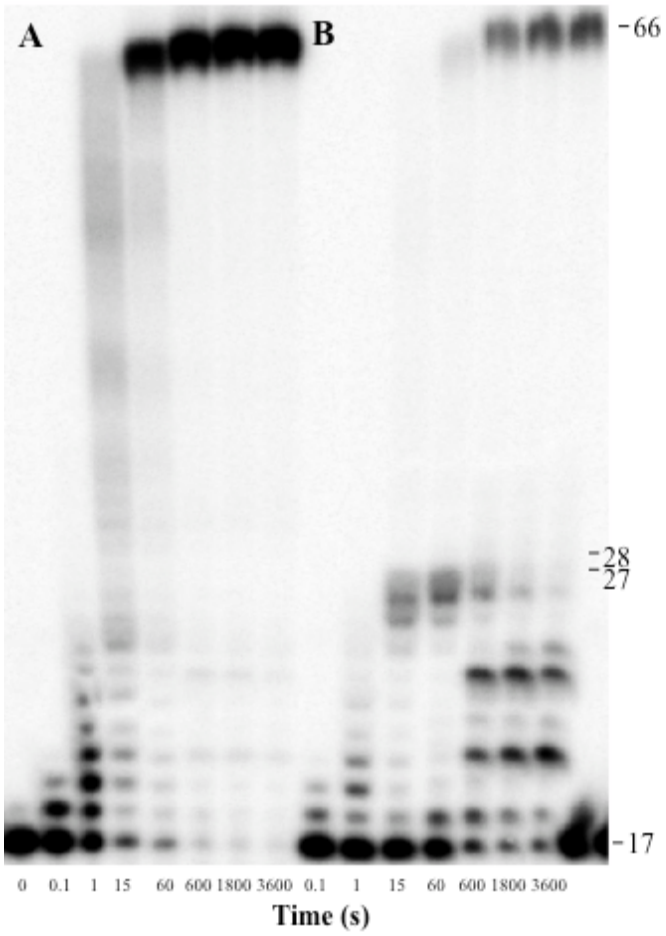

Figure 2. A. Running start assay of hPolκ on 17/77-mer control DNA, B. On 17/77-mer TT DNA. "17" denotes the primer band, "27" T1 of the TT dimer, "28" T2 of the TT dimer, and "66" full length product.

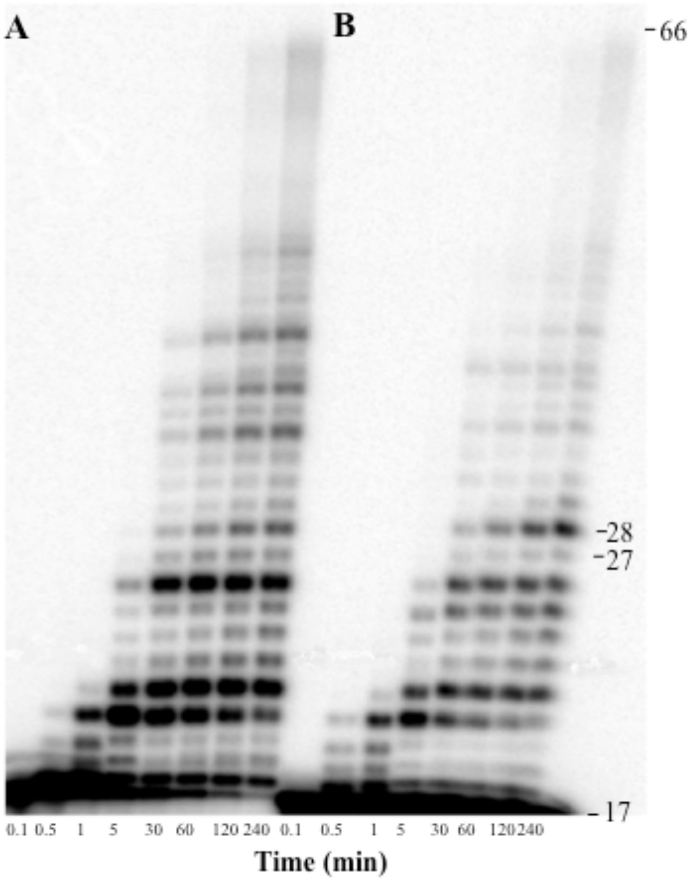

Figure 3. A. Running start assay of hPolι on 17/77-mer control DNA, B. On 17/77-mer TT DNA. "17" denotes the primer band, "27" T1 of the TT dimer, "28" T2 of the TT dimer, and "66" full length product.

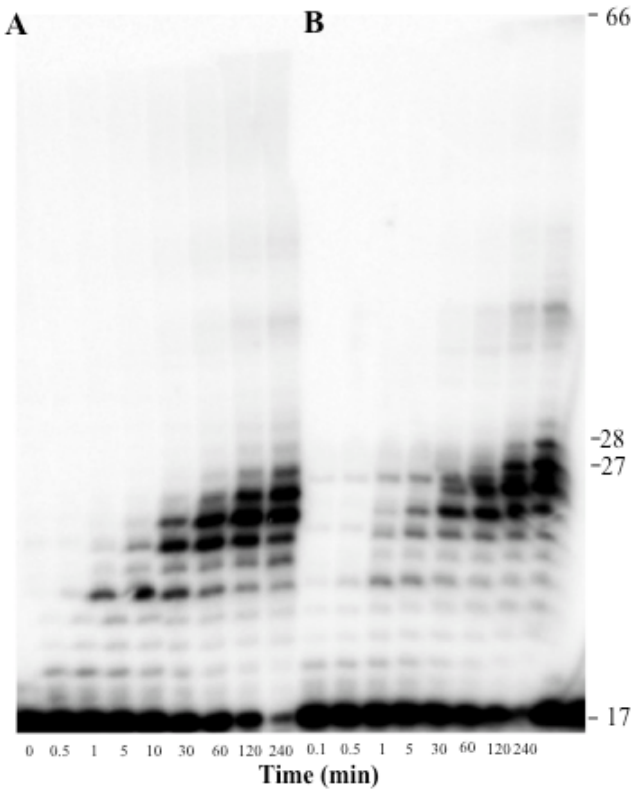

Figure 4. A. Running start assay of hRev1 on 17/77-mer control DNA, B. On 17/77-mer TT DNA. "17" denotes the primer band, T1 and T2 of the TT dimer are indicated and "66" full length product.

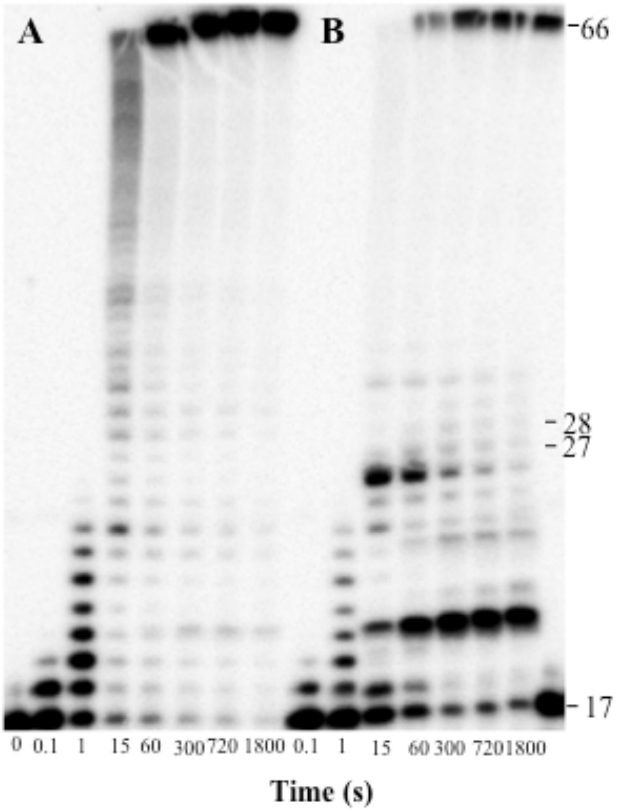

Figure 5. A. Running start assay of Dpo4 on 17/77-mer control DNA, B. On 17/77-mer TT DNA. "17" denotes the primer band, "27" T1 of the TT dimer, "28" T2 of the TT dimer, and "66" full length product.

```
CGGCATCAGCAATGTTG[ACCCAACTCAATGTCGATCCAATGGAGG]CGTGCTGTGCGAGCGGATAGG (2/11)
                  T                                                    (2/11)
                A                 G                                    (2/11)
                     T                                                 (1/11)
                     T   G                                             (1/11)
              C      C       C                                         (1/11)
           A                 G                                        (1/11)
                  G                                                    (1/11)
              A      C    AA      T  T     CCAAT                       (1/11)
```

Figure 6. Mutagenic profile for hPolη's replication of 17/77-mer control DNA. Individual base substitutions (purple), deletions (green), and insertions (blue) are shown. The sequencing window is in bold.

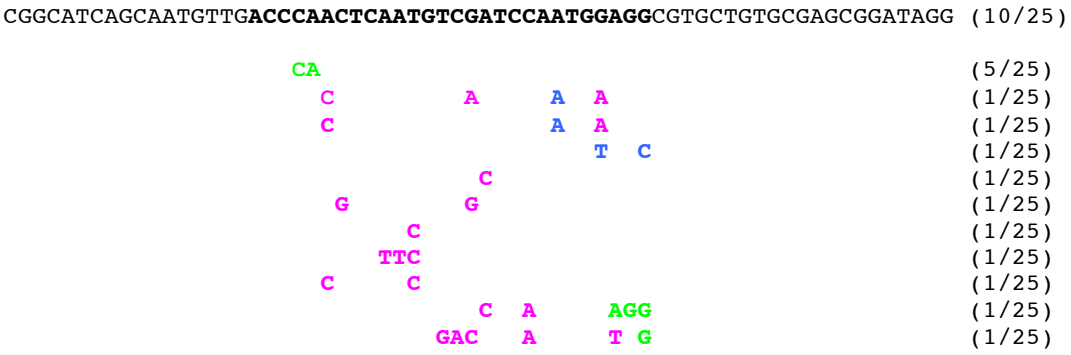

Figure 7. Mutagenic profile for hPolκ's replication of 17/77-mer control DNA. Individual base substitutions (purple), deletions (green), and insertions (blue) are shown. The sequencing window is in bold.

Figure 8. Mutagenic profile for hPolκ's replication of 17/77-mer TT DNA. Individual base substitutions (purple), deletions (green), and insertions (blue) are shown. The sequencing window is in bold. The site of the TT dimer is in red.

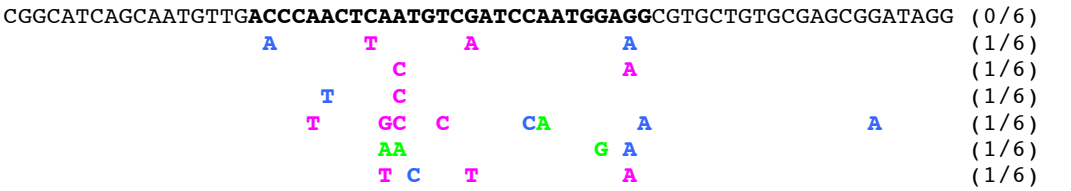

Figure 9. Mutagenic profile for hPolι's replication of 17/77-mer control DNA. Individual base substitutions (purple), deletions (green), and insertions (blue) are shown. The sequencing window is in bold.

Figure 10. Mutagenic profile for hPolι's replication of 17/77-mer TT DNA. Individual base substitutons (purple), deletions (green), and insertions (blue) are shown. The sequencing window is in bold. The site of the TT dimer is in red.

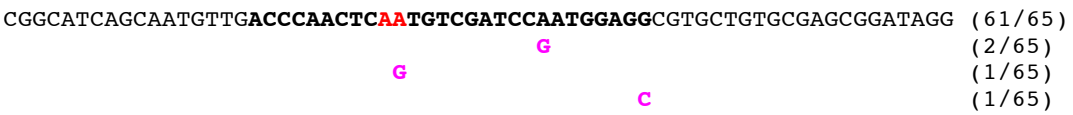

Figure 11. Mutagenic profile for Dpo4's replication of 17/77-mer control DNA. Individual base substitutions (purple), deletions (green), and insertions (blue) are shown. The sequencing window is in bold.

Figure 12. Mutagenic profile for Dpo4's replication of 17/77-mer TT DNA. Individual base substitutions (purple), deletions (green), and insertions (blue) are shown. The sequencing window is in bold. The site of the TT dimer is in red.

Appendix 3

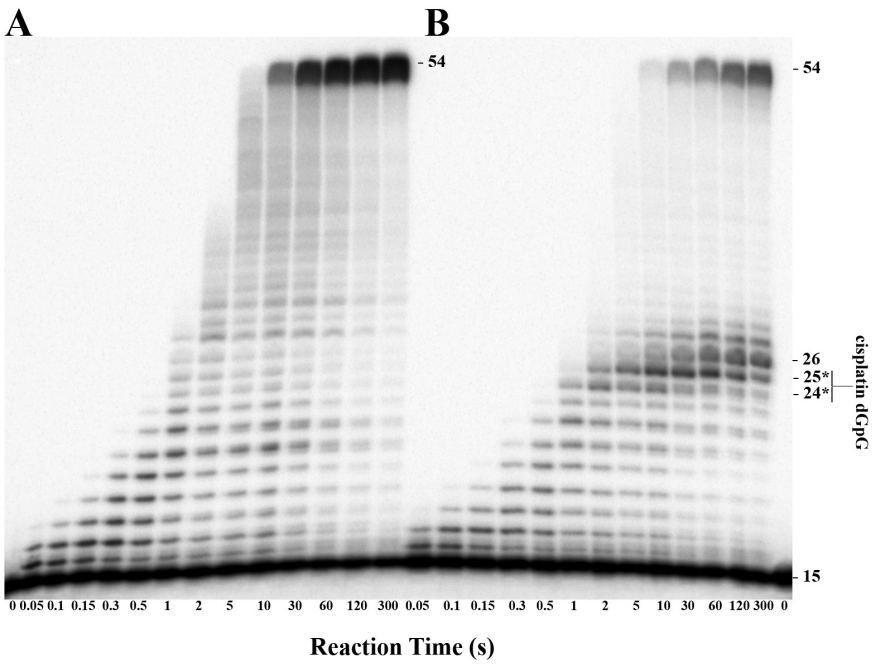

Figure 1. A. Running start assay of hPolη on 15/69-mer control DNA, B. On 15/69-mer CISP DNA. "15" denotes the primer band, "24" G1 of the cisplatin adduct, "25" G2 of the cisplatin adduct, and "54" full length product.

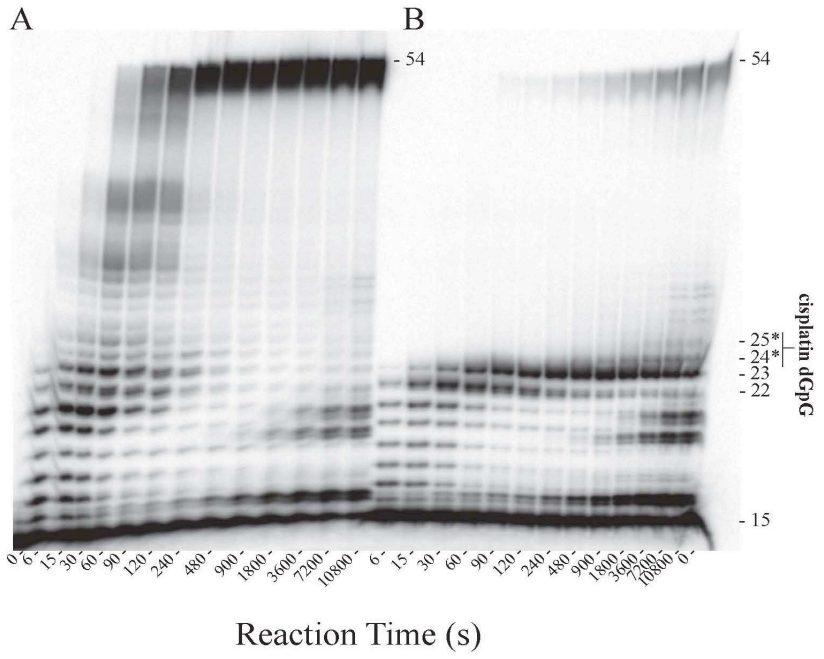

Figure 2. A. Running start assay of hPolκ on 15/69-mer control DNA, B. On 15/69-mer CISP DNA. "15" denotes the primer band, "24" G1 of the cisplatin adduct, "25" G2 of the cisplatin adduct, and "54" full length product.

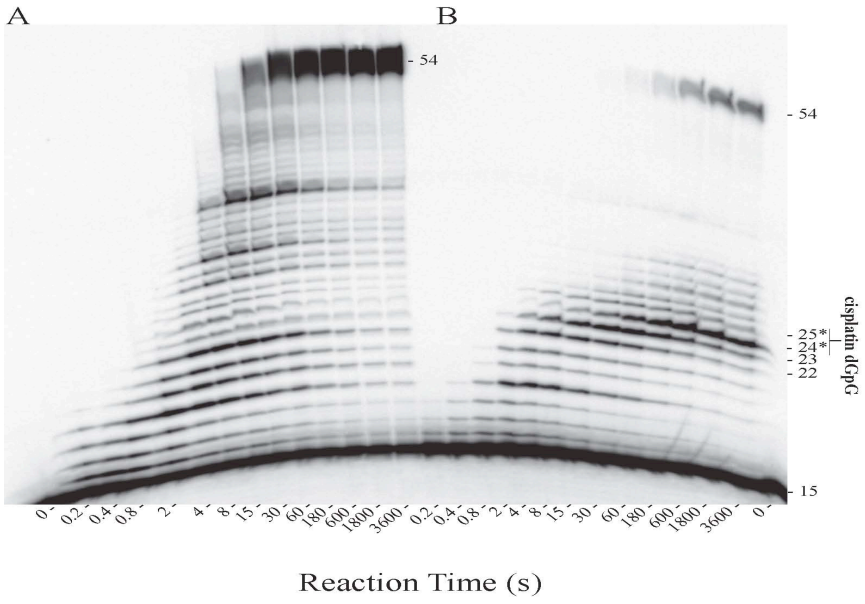

Figure 3. A. Running start assay of Dpo4 on 15/69-mer control DNA, B. On 15/69-mer CISP DNA. "15" denotes the primer band, "24" G1 of the cisplatin adduct, "25" G2 of the cisplatin adduct, and "54" full length product.

Figure 4. Mutagenic profile for hPolκ's replication of 15/69-mer control. Individual base substitutions (dark blue), deletions (light blue), and insertions (orange) are shown. The sequencing window is underlined.

Figure 5. Mutagenic profile for hPolκ's replication of 15/69-mer CISP. Individual base substitutions (dark blue), deletions (light blue), and insertions (orange) are shown. The sequencing window is underlined. The site of the cisplatin-dGpG adduct is in red.

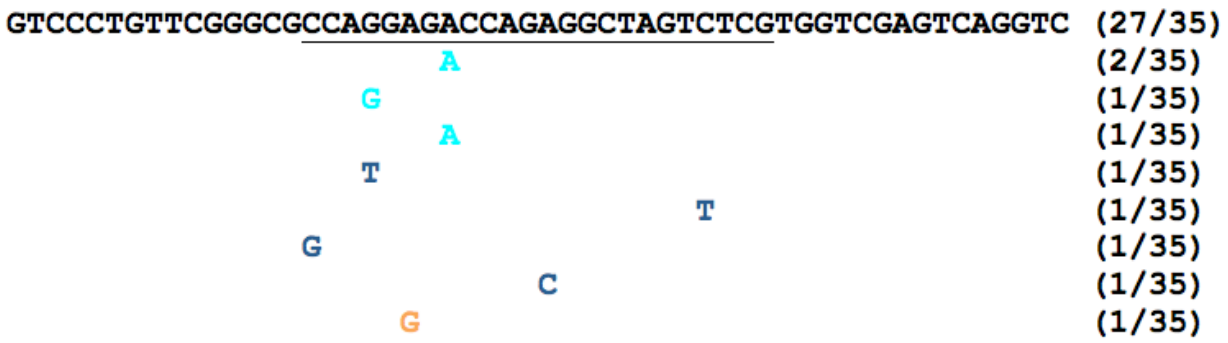

Figure 6. Mutagenic profile for Dpo4's replication of 15/69-mer control. Individual base substitutions (dark blue), deletions (light blue), and insertions (orange) are shown. The sequencing window is underlined.

Figure 7. Mutagenic profile for Dpo4's replication of 15/69-mer CISP. Individual base substitutions (dark blue), deletions (light blue), and insertions (orange) are shown. The sequencing window is underlined. The site of the cisplatin-dGpG adduct is in red.

References

1) Friedberg, E. C. (2003) DNA damage and repair, *Nature* 421, 436-440.

2) Yamtich, J. & Sweasy, J. B. (2010) DNA polymerase Family X: Function, structure, and cellular roles, *Biochimica et Biophysica Acta – Proteins and Proteomics* 1804 (5), 1136-1150.

3) Brown, J. A., Pack, L. R., Sanman, L. E. & Suo, Z. (2011) Efficiency and Fidelity of Human DNA Polymerases λ and β during Gap-Filling DNA Synthesis, *DNA Repair* 10, 24-33.

4) Washington, M. T., Carlson, K. D., Freudenthal, B. D. & Pryor, J. M. (2010) Variations on a theme: eukaryotic Y-family DNA polymerases, *Biochim. Biophys. Acta* 5, 1113-1123.

5) Lindahl, T. & Wood, R. D. (1999) Quality control by DNA repair, *Science. 286*, 1897-905.

6) Frosina, G., Fortini, P., Rossi, O., Carrozzino, F., Raspaglio, G., Cox, L. S., Lane, D. P., Abbondandolo, A. & Dogliotti, E. (1996) Two pathways for base excision repair in mammalian cells, *J Biol Chem. 271*, 9573-8.

7) Garcia-Diaz, M., Bebenek, K., Kunkel, T. A. & Blanco, L. (2001) Identification of an intrinsic 5'-deoxyribose-5-phosphate lyase activity in human DNA polymerase lambda: a possible role in base excision repair, *J Biol Chem. 276*, 34659-63.

8) 7. Sobol, R. W., Horton, J. K., Kuhn, R., Gu, H., Singhal, R. K., Prasad, R., Rajewsky, K. & Wilson, S. H. (1996) Requirement of mammalian DNA polymerase-beta in base-excision repair, *Nature. 379*, 183-6.

9) Asagoshi, K., Liu, Y., Masaoka, A., Lan, L., Prasad, R., Horton, J. K., Brown, A. R., Wang, X. H., Bdour, H. M., Sobol, R. W., Taylor, J. S., Yasui, A. & Wilson, S. H. (2010) DNA polymerase beta-dependent long patch base excision repair in living cells, *DNA Repair (Amst). 9*, 109-19.

10) Aoufouchi, S., Flatter, E., Dahan, A., Faili, A., Bertocci, B., Storck, S., Delbos, F., Cocea,L., Gupta, N., Weill, J. C. & Reynaud, C. A. (2000) Two novel human and mouse DNA polymerases of the polX family, *Nucleic Acids Res. 28*, 3684-93.

11) Shimazaki, N., Yoshida, K., Kobayashi, T., Toji, S., Tamai, K. & Koiwai, O. (2002) Overexpression of human DNA polymerase lambda in E. coli and characterization of the recombinant enzyme, *Genes Cells. 7*, 639-51.

12) Stucki, M., Pascucci, B., Parlanti, E., Fortini, P., Wilson, S. H., Hubscher, U. & Dogliotti, E. (1998) Mammalian base excision repair by DNA polymerases delta and epsilon, *Oncogene* 17(7), 835-43.

13) Garcia-Diaz, M., Bebenek, K., Larrea, A. A., Havener, J. M., Perera, L., Krahn, J. M., Pedersen, L. C., Ramsden, D. A. & Kunkel, T. A. (2009) Template strand scrunching during DNA gap repair synthesis by human polymerase lambda, *Nat Struct Mol Biol. 16*, 967-72.

14) Osheroff, W. P., Jung, H. K., Beard, W. A., Wilson, S. H. & Kunkel, T. A. (1999) The fidelity of DNA polymerase beta during distributive and processive DNA synthesis, *J Biol Chem. 274*, 3642-50.

15) Fiala, K. A., Duym, W. W., Zhang, J. & Suo, Z. (2006) Up-regulation of the fidelity of human DNA polymerase lambda by its non-enzymatic proline-rich domain, *J Biol Chem.281*, 19038-44.

16) Garcia-Diaz, M., Bebenek, K., Gao, G., Pedersen, L. C., London, R. E. & Kunkel, T. A. (2005) Structure-function studies of DNA polymerase lambda, *DNA Repair (Amst). 4*, 1358-67.

17) Garcia-Diaz, M., Bebenek, K., Krahn, J. M., Kunkel, T. A. & Pedersen, L. C. (2005) A closed conformation for the Pol lambda catalytic cycle, *Nat Struct Mol Biol. 12*, 97-98.

18) Sawaya, M. R., Prasad, R., Wilson, S. H., Kraut, J. & Pelletier, H. (1997) Crystal structures of human DNA polymerase beta complexed with gapped and nicked DNA: evidence for aninduced fit mechanism, *Biochemistry. 36*, 11205-15.

19) Chan, K. K., Zhang, Q. M. & Dianov, G. L. (2006) Base excision repair fidelity in normal and cancer cells, *Mutagenesis. 21*, 173-8.

20) Liu, Y., Beard, W. A., Shock, D. D., Prasad, R., Hou, E. W. & Wilson, S. H. (2005) DNA polymerase beta and flap endonuclease 1 enzymatic specificities sustain DNA synthesis for long patch base excision repair, *J Biol Chem. 280*, 3665-74.

21) Podlutsky, A. J., Dianova, II, Podust, V. N., Bohr, V. A. & Dianov, G. L. (2001) Human DNA polymerase beta initiates DNA synthesis during long-patch repair of reduced AP sites in DNA, *Embo J. 20*, 1477-82.

22) Parlanti, E., Pascucci, B., Terrados, G., Blanco, L. & Dogliotti, E. (2004) Aphidicolin resistant and -sensitive base excision repair in wild-type and DNA polymerase beta-defective mouse cells, *DNA Repair (Amst). 3*, 703-10.

23) Duym, W. W., Fiala, K. A., Bhatt, N. & Suo, Z. (2006) Kinetic effect of a downstream strand and its 5'-terminal moieties on single nucleotide gap-filling synthesis catalyzed by human DNA polymerase lambda, *J Biol Chem. 281*, 35649-55.

24) Stary, A., Kannouche, P., Lehmann, A. R. & Sarasin, A. (2003) Role of DNA Polymerase h in the UV Mutation Spectrum in Human Cells, *J Biol. Chem. 278*, 18767-18775.

25) Sherrer, S. M., Fiala, K. A., Fowler, J. D., Newmister, S. A., Pryor, J. M. & Suo, Z. (2011) Quantitative Analysis of the Efficiency and Mutagenic Spectra of Abasic Lesion Bypass Catalyzed by Human Y-family DNA Polymerases, *Nucleic Acids Research 39*, 609-622.

26) Thoma, F. (1999) Light and dark in chromatin repair: repair of UV-induced DNA lesions by photolyase and nucleotide excision repair, *The EMBO Journal 18*, 6585-6598.

27) Wang, Y., Woodgate, R., McManus, T. P., Mead, S., McCormick, J. J. and Maher, V. M. (2007) Evidence that in xeroderma pigmentosum variant cells, which lack DNA polymerase eta,

DNA polymerase iota causes the very high frequency and unique spectrum of UV-induced mutations, *Cancer Res. 67*, 3018-3026.

28) Kusumoto, R., Masutani, C., Shimmyo, S., Iwai, S. and Hanaoka, F. (2004) DNA binding properties of human DNA polymerase eta: implications for fidelity and polymerase switching of translesion synthesis, *Genes Cells 9*, 1139-1150.

29) Park, H. J., Zhang, K., Ren, Y., Nadji, S., Sinha, N., Taylor, J. S. & Kang, C. (2002) Crystal structure of a DNA decamer containing a *cis-syn* thymine dimer, *PNAS 99*, 15965-15970.

30) Biertumpfel, C., Zhao, Y., Kondo, Y., Ramón-Maiques, S., Gregory, M., Lee, J. Y., Masutani, C., Lehmann, A. R., Hanaoka, F. & Yang, W. (2010) Structure and mechanism of human DNA polymerase eta, *Nature 465*, 1044-1048.

31) Johnson, R. E., Prakash, L. & Prakash, S. (2005) Distinct mechanisms of *cis-syn* thymine dimer bypass by Dpo4 and DNA polymerase η, *PNAS 102*, 12359-12364.

32) Tissier, A., Frank, E. G., McDonald, J. P., Iwai, S., Hanaoka, F. & Woodgate, R. (2000) Misinsertion and bypass of thymine-thymine dimers by human DNA polymerase ι, *The EMBO Journal 19*, 5259-5266.

33) Silverstein, T. D., Johnson, R. E., Jain, R., Prakash, L., Prakash, S. & Aggarwal, Aneel. (2010) Structural basis for the suppression of skin cancers by DNA polymerase η, *Nature 465*, 1039-1043.

34) Wolfle, W. T., Washington, M. T., Kool, E. T., Spratt, T. E., Helquist, S. A., Prakash, L. & Prakash, S. (2005) Evidence for a Watson-Crick Hydrogen Bonding Requirement in DNA Synthesis by Human DNA Polymerase κ, *Molecular and Cellular Biology 25*, 7137-7143.

35) Vasquez-Del Carpio, R., Silverstein, T. D., Lone, S., Johnson, R. E., Prakash, L., Prakash, S. & Aggarwal, A. K. (2011) Role of Human DNA Polymerase κ in Extension Opposite from a cis-syn Thymine Dimer, *J Mol Bio 408*, 252-261.

36) Washington, M. T., Johnson, R. E., Prakash, L. & Prakash, S. (2004) Human DNA Polymerase ι Utilizes Different Nucleotide Incorporation Mechanisms Dependent on the Template Base, *Molecular and Cellular Biology 24*, 936-943.

37) Brown, J. A., Fowler, J. D. & Suo, Z. (2010) Kinetic Basis of Nucleotide Selection Employed by a Protein Template-Dependent DNA Polymerase, *Biochemistry 49*, 5504-5510.

38) Hicks, J. K., Chute, C. L., Paulsen, M. T., Ragland, R. L., Howlett, N. G., Guéranger, Q., Glover, T. W. & Canman, C. E. (2010) Differential Roles for DNA Polymerases Eta, Zeta, and REV1 in Lesion Bypass of Intrastrand versus Interstrand DNA Cross-Links, *Molecular and Cellular Biology 30,* 1217-1230.

39) Ling, H., Boudsocq, F., Woodgate, R. & Yang, W. (2001) Crystal structure of a Y-Family DNA Polymerase in Action: A Mechanism for Error-Prone and Lesion-Bypass Replication, *Cell 107,* 91-102.

40) Fiala, K. A. & Suo, Z. (2007) Sloppy Bypass of an Abasic Lesion Catalyzed by a Y-family DNA Polymerase, *J. Biol. Chem. 282,* 8199-8206.

41) Brown, J. A., Newmister, S. A., Fiala, K. A., and Suo, Z. (2008) Mechanism of double-base lesion bypass catalyzed by a Y-family DNA polymerase, *Nucleic Acids Research 36*, 3867-3878.

42) Takahara P. M., Rozenweig A. C., Frederick C. A., Lippard S. J. (1995) Crystal structure of double-stranded DNA containing the major adduct of the anticancer drug cisplatin, *Nature 377,* 649–652.

43) Albertella, M. R., Green, C. M., Lehmann, A. R. & O'Connor, M. J. (2005) A role for polymerase eta in the cellular tolerance to cisplatin-induced damage, *Cancer Res 65,* 97999806.

44) Alt, A., Lammens, K., Chiocchini, C., Lammens, A., Pieck, J. C., Kuch, D., Hopfner, K.-P. & Carell, T. (2007) Bypass of DNA Lesions Generated During Anticancer Treatment with Cisplatin by DNA Polymerase η. *Science 9*, 967-970.

45) Chaney, S. G., Campbell, S. L., Bassett, E. & Wu, Y. (2005). Recognition and processing of cisplatin- and oxaliplatin-DNA adducts. *Crit. Rev. Oncol. Hematol. 53,* 3-11.

46) Masutani, C., Kusumoto, R., Iwai, S. & Hanaoka, F. (2000) Mechanisms of accurate translesion synthesis by human DNA polymerase η. *EMBO Journal 19*, 3100-3109.

47) Wolfle, W. T., Washington, M. T., Prakash, L. & Prakash, S. (2003) Human DNA polymerase kappa uses template-primer misalignment as a novel means for extending mispaired termini and for generating single-base deletions, *Genes Dev 17,* 2191-2199.

48) Wong, J. H, Brown, J. A., Suo, Z., Blum, P., Nohmi, T. & Ling, H. (2010) Structural insight into dynamic bypass of the major cisplatin-DNA adduct by Y-family polymerase Dpo4, *EMBO Journal 29,* 2059-2069.

49) Wu, Y., Wilson, R. C. & Pata, J. (2011) The Y-Family DNA Polymerase Dpo4 Uses a Template Slippage Mechanism to Create Single-Base Deletions, *J. Bact. 193,* 2630-2636.